Experimental Investigation on Mechanical Properties of Nanospring Thin Films Fabricated by Glancing Angle Deposition Technique

Chen Shaoguang

March 2017

Contents

Chapter 1 Introduction

In recent decades, the nanostructured thin films which consist of discretely nano-sized three-dimensional elements have been attracting a great deal of attention because of their characteristic physical properties, such as alterable thermal conductivity [1,2], anisotropic magnetic property [3-5], tunable refractive index [6-9] and excellent mechanical properties [10-16]. These outstanding features stem from the unique geometry of the micro- and nano-structures, which could strongly affect various physical properties of thin film [17-20]. Among these nanostructured thin films, the thin film composed of helical shaped nanosprings is a representative one due to its large deformation reversibility and the anisotropy of mechanical behaviors [13, 15, 21, 22]. Because of these unique mechanical properties, nanospring thin films have shown great potential in improving the sensitivity and reliability of advanced electronic devices [23-26].

Until now, several methodologies including photolithography method [27, 28], metalorganic chemical vapor deposition [29, 30] and vapor-liquid-solid growth [31, 32] have been developed to fabricate thin films consisting of discretely nano-sized three-dimensional elements. However, it should be noted that it is extremely difficult to precisely control the geometric configuration of nano-sized elements in these nanostructured thin films by using aforementioned methods. Recently, the glancing angle deposition (GLAD) method is developed to fabricate thin films with various shaped nano-elements on a substrate [33-38], such as slant, zigzag and helical

nano-elements. GLAD is intrinsically a physical vapor deposition technique with high efficiency for bottom-up nanofabrication of the thin film consisting of helical nanosprings. This method combines oblique angle deposition (OAD) with substrate motion control, which can produce different nano-sized columnar films with controlled shapes and density [39-42]. Figure 1 shows the process of fabricating a nanospring thin film using the GLAD technique. The trajectory of incoming vapor atoms have a large incident angle with respect to the substrate surface normal. These atoms make numerous islands at the early stage of deposition. Once islands are formed, successive atoms cannot reach the other side by the oblique deposition due to the shadow effect. Thus, each island grows in one direction and forms a slanted nano-bar. As the substrate rotates during the deposition, the growth direction is twisted, and this results in bars with helical shape.

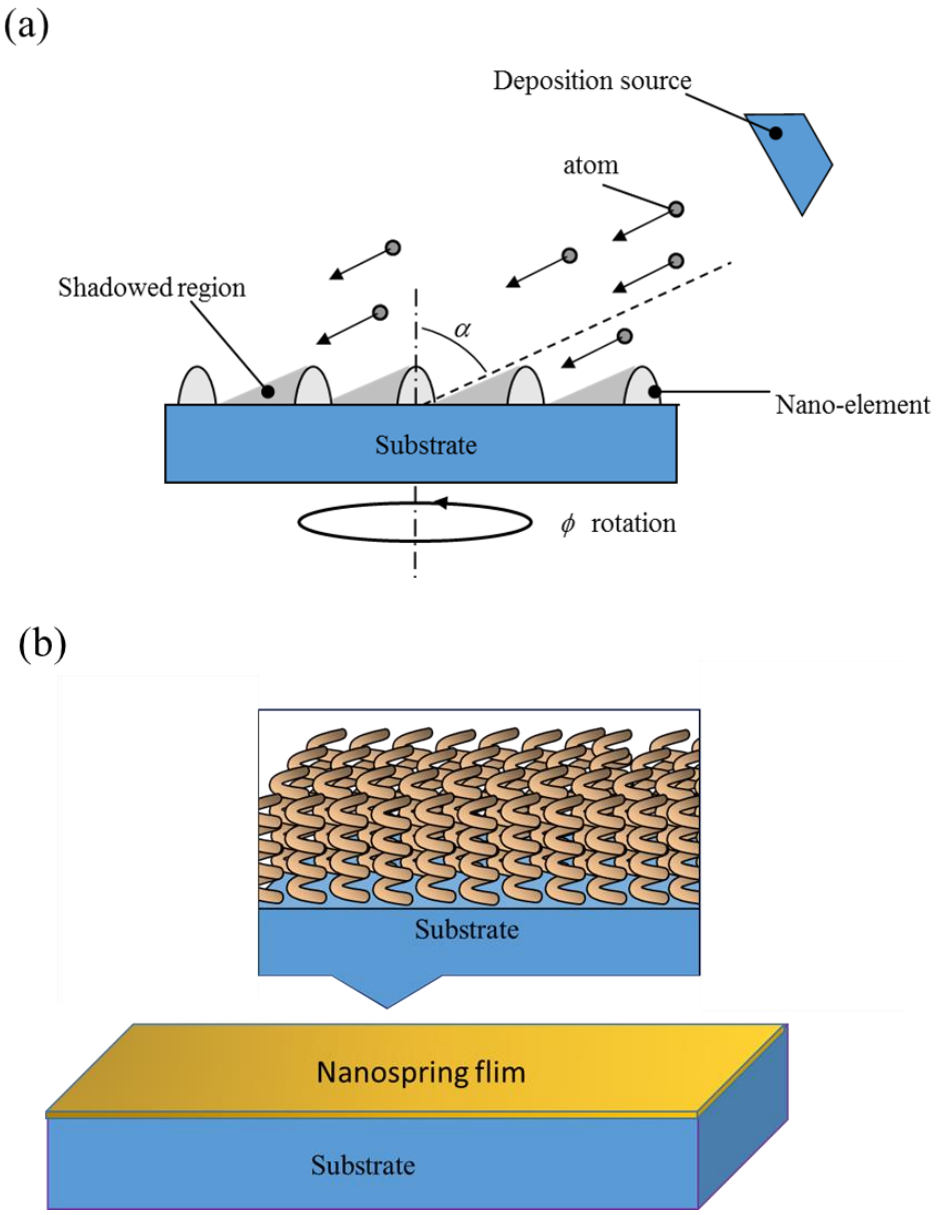

Fig.1 (a) Schematic depiction of nanospring thin film growth by glancing angle deposition (GLAD) technique. (b) The nanostructured thin film consisted of numerous helical nanospring.

Because nanospring thin films are composed of distinctly separated nano-elements rather than being a continuous solid film, entirely different and novel mechanical behaviors are expected. For nanospring thin film, its mechanical properties usually possess strong anisotropy due to the geometrical anisotropy of nanospring. Since the nanospring could easily deform in the transverse direction compared with the longitudinal one, the thin film of arrayed nanosprings is expected to show strong anisotropy in deformation. Hirakata et al. found that the nanospring thin films showed strong characteristic anisotropy that the solid one could hardly attain, and the stiffness and its anisotropy strongly depended on nanospring shape [43, 44]. In addition, the mechanical properties of nanospring thin films show great dependency on the morphology of helical nano-elements. For example, the anisotropy can be controlled by the height of nanospring and the helical spring could offer large elongation than column which make nanospring film could have giant elastic limit [45, 46]. Very recent studies by Sumigawa et al. [13, 14] revealed that by inserting a nanospring thin film at the bi-material interface in multi-layered materials, the stress singularity at the interface edge was relaxed and thus interfacial delamination between dissimilar materials was prevented. This remarkable characteristic of the nanospring thin film could be used to protect the device from malfunction induced by interface delamination.

Because the mechanical behavior of the helical nanospring can be significantly modified by the density (the average distance between adjacent nanosprings), geometrical configuration (different turns) and dimension (height and wire diameter) of the nanosprings [11, 39], a desired nanospring thin film with certain mechanical response could be achieved by controlling the GLAD fabrication process. Although

nanospring thin films with different geometric configurations have already been developed, due to experimental difficulties in applying load and precise measurement of minute parameters, mechanical properties of both thin film as well as single individual nanospring have not been clearly clarified. Therefore, to insure the reliability of components constructed by nanospring thin film in further applications, it is of critical importance to clearly investigate the deformation and fracture behaviors of nanospring thin film.

High electrical conductivity is an intrinsic requirement for the further application of nanospring thin films in advanced electronic devices. Copper (Cu) and aluminum (Al) have been widely adopted in electronic devices due to their well conductivity. However, it should be noted that Cu [35] and Al [47] are low-melting metals. This results in apparent difficulties to fabricate nanospring thin films with precise geometric shapes by using GLAD technique induced by the high adatom mobility , because nanosprings are grown on a substrate by limited adatom diffusion and atomic-scale self-shadowing effect [48, 49], which prevents the vapor flux from reaching the regions behind early nuclei. Although nano-whiskers of Cu and Al have been formed on planar morphologies at a high temperature, the shape and the distribution of nano-whiskers were completely uncontrollable [50, 51]. Thus, it is difficult to achieve a precise geometric configuration of arranged nanoelements of low-melting metals in nanostructured thin films by using a common GLAD method. To suppress the high atom mobility of low-melting metal, holding the substrate at low temperature is a possible method. However, due to experimental difficulties, the effect of substrate temperature on the formation of nanospring thin films have not been clearly investigated, and critical substrate

temperature for forming nanosprings with different morphologies has not been clarified.

For the design of microelectronic devices, not only the electrical conductivity but also the yielding behavior of metals should be carefully considered, because it is one of important properties avoiding the malfunction during actual application. Therefore, in order to assure the reliability of components consisting of nanospring thin film, it is necessary to precisely evaluate the yielding behavior of nanospring thin film. It is well known that nanoscale material possesses much higher yield stress than that of its bulk counterpart due to Hall-Petch mechanism [52-55]. Thus, the yield stress of nanospring thin film constructed by numerous individual nano-sized elements is expected to be significantly increased. In addition, the helical spring has been found to possess much lower vertical stiffness than that of bar and zigzag springs, and thus the helical shape can sustain large reversible deformation [56]. As a results, the shape of discrete nanospring also strongly affects the elastic limit of nanospring thin film. Up to now, although many experimental investigations have been conducted to clarify the mechanical properties of nanospring thin films, the study focus is mainly placed on the anisotropy of stiffness and the shape effect of various nanoelements on the mechanical properties [14, 21, 37, 39]. There has been no study on the yielding behavior of nanospring film, and effect of the size and the shape of individual nano-sized spring on the elastic limit of whole thin film has not been investigated.

Because of difficulties in applying loading to nanospring thin film and precise measurement of minute quantities, a few experimental studies have been carried out for the compression testing of nanospring films by means of an atomic force microscope

(AFM) combine with a nano-indentation device [11, 13-15, 57]. However, since the indentation tip is much larger than the size of a single nanospring, the load is applied on numerous nanosprings and thus obtained mechanical properties represent the average. Because the shape of nanospring fabricated by GLAD technique is not exactly same duo to the random atom diffusion, it is difficult to clearly understand the mechanism and mechanics of deformation/fracture characteristics of nanospring thin films in detail by these experiments. On the other hand, several recent experimental studies were performed on an individual nanospring by compression tests [58-60]. However, only mechanical properties in the elastic region were evaluated because the adjacent nanosprings block the deformation of target one. Thus, it is necessary to develop a tension method to investigate the mechanical property of the single nanospring under large deformation especially for fracture behavior. Moreover, for experiments using AFM or nano-indentation devices, the obtained information from the *ex situ* experiments is limited by either a lack of quantitative stress-strain information or by the incapability of monitoring the evolving the local and global deformation process. So, the *in situ* experimental methodology using electron microscopy is required to obtain details on the deformation and fracture processes for the nanospring.

In this dissertation work, thin films consisting of helical shaped nanospring are fabricated by GLAD technique with the precise control of substrate temperature, and the mechanical properties of the nanospring thin film as well as the individual nanospring are investigated by experimental investigation and numerical analysis. The thesis is organized as follows.

In chapter 2, a novel experimental device is developed to precisely control the substrate temperature during glancing angle deposition and thin films consisting of low-melting Cu and Al nanosprings with helical shape are successfully fabricated. Moreover, the effect of substrate temperature on the geometrical configuration of nanospring thin films is also investigated.

In chapter 3, a thin film composed of nickel helical nanosprings is fabricated, and its yielding behavior is characterized by loading tests using an atomic force microscope (AFM). In addition, the effect of size and shape of the single nanospring on the elastic limit of the thin film is investigated by finite element method (FEM) analysis.

In chapter 4, an *in situ* tensile method inside a scanning electron microscopy (SEM) is developed for single silicon nanospring prepared by GLAD technique. Experiments are conducted for several nanosprings to clarify the difference in the deformation and fracture properties among individual nano-element extracted from the same film and elucidate the mechanism in detail.

In chapter 5, the obtained results from chapter 2 to chapter 4 are summarized.

References in chapter 1

[1] Plawsky, J. L., et al., "Dielectric Films for Advanced Microelectronics." Wiley and Sons, London (2007) Ch. 4, 137-198.

[2] Jain, A., Rogojevic, S., Ponoth, S., Gill, W. N., Plawsky, J. L., Simonyi, E., and Ho, P. S. "Processing dependent thermal conductivity of nanoporous silica xerogel films." Journal of applied physics, 91.5 (2002), 3275-3281.

[3] Knorr T G, Hoffman R W. "Dependence of geometric magnetic anisotropy in thin iron films. Physical Review." 1959, 113(4): 1039.

[4] Broughton, J. N., and M. J. Brett. "Electrochemical capacitance in manganese thin films with chevron microstructure." Electrochemical and solid-state letters 5.12 (2002): 279-282.

[5] Smith D O. "Anisotropy in permalloy films." Journal of Applied Physics, 1959, 30(4): 264-265.

[6] Schubert M F, Xi J Q, Kim J K, et al. "Distributed Bragg reflector consisting of high-and low-refractive-index thin film layers made of the same material." Applied physics letters, 2007, 90(14): 141115.

[7] Xi J Q, Schubert M F, Kim J K, et al. "Optical thin-film materials with low refractive index for broadband elimination of Fresnel reflection. " Nature photonics, 2007, 1(3): 176-179.

[8] Kim J K, Chhajed S, Schubert M F, et al. "Light−extraction enhancement of GaInN light−emitting diodes by graded−refractive−index indium tin oxide anti−reflection

contact." Advanced materials, 2008, 20(4): 801-804.

[9] Poxson D J, Schubert M F, Mont F W, et al. "Broadband omnidirectional antireflection coatings optimized by genetic algorithm. " Optics letters, 2009, 34(6): 728-730.

[10] Smith, D. O., Cohen, M. S., and Weiss, G. P. "Oblique-incidence anisotropy in evaporated Permalloy films." Journal of Applied Physics, 31.10 (1960), 1755-1762.

[11] Seto, Mary W., Brian Dick, and Michael J. Brett. "Microsprings and microcantilevers: studies of mechanical response." Journal of Micromechanics and Microengineering 11.5 (2001): 582.

[12] Zhang, Guigen, and Yiping Zhao. "Mechanical characteristics of nanoscale springs." Journal of applied physics 95.1 (2004): 267-271.

[13] Sumigawa, Takashi, et al. "Disappearance of stress singularity at interface edge due to nanostructured thin film." Engineering Fracture Mechanics 75.10 (2008): 3073-3083.

[14] Sumigawa T, Sueda T, Futamura Y, et al. "Effect of interface layer consisting of nanosprings on stress field near interface edge. Engineering Fracture Mechanics." 2009, 76(9): 1336-1344.

[15] Hirakata H, Matsumoto S, Takemura M, et al. "Anisotropic deformation of thin films comprised of helical nanosprings." International journal of solids and structures, 2007, 44(11): 4030-4038.

[16] Harris, K. D., Brett, M. J., Smy, T. J., and Backhouse, C. "Microchannel surface

area enhancement using porous thin films." Journal of the Electrochemical Society, 147.5 (2000), 2002-2006.

[17] Plawsky J L, Kim J K, Schubert E F. "Engineered nanoporous and nanostructured films."Materials Today, 2009, 12(6): 36-45.

[18] Steele J J, Brett M J. "Nanostructure engineering in porous columnar thin films: recent advances." Journal of Materials Science: Materials in Electronics, 2007, 18(4): 367-379.

[19] Hawkeye M M, Brett M J. "Glancing angle deposition: fabrication, properties, and applications of micro-and nanostructured thin films." Journal of Vacuum Science & Technology A, 2007, 25(5): 1317-1335.

[20] Ge L, Sethi S, Ci L, et al. "Carbon nanotube-based synthetic gecko tapes." Proceedings of the National Academy of Sciences, 2007, 104(26): 10792-10795.

[21] Liu, D-L., et al. "Mechanics of patterned helical Si springs on Si substrate." Journal of nanoscience and nanotechnology 3.6 (2003): 492-495.

[22] Gaire, C., Ye, D. X., Lu, T. M., Wang, G. C., and Picu, R. C. "Deformation of amorphous silicon nanostructures subjected to monotonic and cyclic loading." Journal of Materials Research, 23.2 (2008), 328-335.

[23] Majcherek, S., Aman, A., and Fochtmann, J. "A MEMS sensor for microscale force measurements." Journal of Micromechanics and Microengineering, 26.2 (2016), 025013.

[24] Shoaib, M., Hisham, N., Basheer, N., and Tariq, M. "Frequency and displacement

analysis of electrostatic cantilever-based MEMS sensor." Analog Integrated Circuits and Signal Processing, (2016) 1-11.

[25] Wu, C. H., Kang, D., Chen, P. H., and Tai, Y. C. "MEMS thermal flow sensors. Sensors and Actuators A: Physical." 241 (2016), 135-144.

[26] Kose, T., Azgin, K., and Akin, T. "Design and fabrication of a high performance resonant MEMS temperature sensor." Journal of Micromechanics and Microengineering, 26.4 (2016), 045012.

[27] Shi, R., Huang, C., Zhang, L., Amini, A., Liu, K., Shi, Y. and Cheng, C. (2016). "Three Dimensional Sculpturing of Vertical Nanowire Arrays by Conventional Photolithography." *Scientific reports*, *6*.

[28] Kathuria, Himanshu, et al. "Polymeric Microneedle Array Fabrication by Photolithography." *JoVE (Journal of Visualized Experiments)* 105 (2015): 52914-52914.

[29] Hung, S.C., et al. "Shell buckling behavior investigation of individual gallium nitride hollow nanocolumn." *Applied Physics A* 84.4 (2006): 439-443.

[30] Zhang, B. P., et al. "Optical properties of ZnO rods formed by metalorganic chemical vapor deposition." *Applied Physics Letters* 83.8 (2003): 1635-1637.

[31] Kodambaka, S., Tersoff, J., Reuter, M. C., & Ross, F. M. (2006). "Diameter-independent kinetics in the vapor-liquid-solid growth of Si nanowires." *Physical review letters*, *96*(9), 096105.

[32] Zhu, Y., Xu, F., Qin, Q., Fung, W. Y., and Lu, W. (2009). "Mechanical properties of

vapor−liquid−solid synthesized silicon nanowires." *Nano letters*, *9*(11), 3934-3939.

[33] Robbie K, Brett M J. "Sculptured thin films and glancing angle deposition: Growth mechanics and applications." Journal of Vacuum Science & Technology A, 1997, 15(3): 1460-1465.

[34] Robbie, K., J. C. Sit, and M. J. Brett. "Advanced techniques for glancing angle deposition." Journal of Vacuum Science & Technology B 16.3 (1998): 1115-1122.

[35] Harris, Kenneth D., Jeremy C. Sit, and Michael J. Brett. "Fabrication and optical characterization of template-constructed thin films with chiral nanostructure." IEEE transactions on nanotechnology 1.3 (2002): 122-128.

[36] Steele, John J., and Michael J. Brett. "Nanostructure engineering in porous columnar thin films: recent advances." Journal of Materials Science: Materials in Electronics 18.4 (2007): 367-379.

[37] Seto, M. W., et al. "Mechanical response of thin films with helical microstructures." Journal of Vacuum Science & Technology B 17.5 (1999): 2172-2177.

[38] Seto, Mary W., Brian Dick, and Michael J. Brett. "Microsprings and microcantilevers: studies of mechanical response." Journal of Micromechanics and Microengineering 11.5 (2001): 582.

[39] Li, B., Luo, Z., Ho, P. S., and Lu, T. M. (2003, September). "Nanoindentation Study of the Mechanical Behavior of Silicon Nano-springs." In AIP Conference Proceedings (pp. 525-532). IOP INSTITUTE OF PHYSICS PUBLISHING LTD.

[40] Hawkeye, Matthew M., and Michael J. Brett. "Glancing angle deposition:

fabrication, properties, and applications of micro-and nanostructured thin films." *Journal of Vacuum Science & Technology A* 25.5 (2007): 1317-1335.

[41] Fan, J. G., et al. "The effect of the shape of nanorod arrays on the nanocarpet effect." *Nanotechnology* 19.4 (2008): 045713.

[42] ZHAO, Yiping, et al. "Designing nanostructures by glancing angle deposition." In: *Optical Science and Technology, SPIE's 48th Annual Meeting*. International Society for Optics and Photonics, (2003): 59-73.

[43] Hirakata, Hiroyuki, et al. "Anisotropic deformation of thin films comprised of helical nanosprings." *International journal of solids and structures* 44.11 (2007): 4030-4038.

[44] Kesapragada S V, Gall D. "Anisotropic broadening of Cu nanorods during glancing angle deposition." Applied physics letters, 2006, 89(20): 203121.

[45] Smith, D. O., Cohen, M. S., and Weiss, G. P. "Oblique-incidence anisotropy in evaporated Permalloy films." Journal of Applied Physics, 31.10 (1960), 1755-1762.

[46] Haque, M. A., and Saif, M. T. A. "In-situ tensile testing of nano-scale specimens in SEM and TEM. Experimental Mechanics." 42.1(2002), 123-128.

[47] Dick, B., Brett, M. J., and Smy, T. "Controlled growth of periodic pillars by glancing angle deposition." Journal of Vacuum Science & Technology B, 21.1(2003), 23-28.

[48] Messier, Russell, Vijayakumar C. Venugopal, and Paul D. Sunal. "Origin and evolution of sculptured thin films." Journal of Vacuum Science and Technology A

18.4 (2000): 1538-1545.

[49] Krug, Joachim. "Origins of scale invariance in growth processes." Advances in Physics 46.2 (1997): 139-282.

[50] Suzuki, M., Nagai, K., Kinoshita, S., Nakajima, K., Kimura, K., Okano, T., and Sasakawa, K.. "Vapor phase growth of Al whiskers induced by glancing angle deposition at high temperature." Applied physics letters, 89.13 (2006), 133103.

[51] Mukherjee, S., Zhou, C. M., and Gall, D. "Temperature-induced chaos during nanorod growth by physical vapor deposition." Journal of Applied Physics, 105.9 (2009), 094318.

[52] Haque, M. A., and Saif, M. T. A. "In-situ tensile testing of nano-scale specimens in SEM and TEM." Experimental Mechanics, 42.1(2002), 123-128.

[53] Uchic, M. D., Dimiduk, D. M., Florando, J. N., and Nix, W. D. "Sample dimensions influence strength and crystal plasticity." Science, 305. 5686 (2004), 986-989.

[54] Pande, C. S., Masumura, R. A., and Armstrong, R. W. "Pile-up based Hall-Petch relation for nanoscale materials." Nanostructured materials, 2.3 (1993), 323-331.

[55] Cotterell, B. "Cleavage Fracture of Polycrystalline Aggregates." (1963): 161-161.

[56] Chen, X., Zhang, S., Dikin, D. A., Ding, W., Ruoff, R. S., Pan, L., and Nakayama, Y. "Mechanics of a carbon nanocoil." Nano Letters, 3.9 (2003), 1299-1304.

[57] Lintymer J, Martin N, Chappé J M, et al. "Nanoindentation of chromium zigzag thin films sputter deposited." Surface and Coatings Technology, 2005, 200(1): 269-272.

[58] Gaire, C., Ye, D. X., Lu, T. M., Wang, G. C., and Picu, R. C. "Deformation of amorphous silicon nanostructures subjected to monotonic and cyclic loading." Journal of Materials Research, 23.2 (2008), 328-335.

[59] Gaire, C., Ye, D. X., Tang, F., Picu, R. C., Wang, G. C., and Lu, T. M. "Mechanical testing of isolated amorphous silicon slanted nanorods." Journal of nanoscience and nanotechnology, 5.11 (2005), 1893-1897.

[60] Liu, D-L., et al. "Mechanics of patterned helical Si springs on Si substrate." Journal of nanoscience and nanotechnology 3.6 (2003): 492-495.

Chapter 2 Substrate Temperature Control for the Formation of Metal Nanosprings

2.1 Introduction

Glancing angle deposition (GLAD) is a physical vapor deposition technique in which the deposition angle and in-plane direction of the substrate are changed during deposition, which enable us to fabricate nanostructured thin film [1-5]. By controlling the deposition angle, the rotation speed of substrate and the growth rate, thin films composed of different nano-sized structures with various shapes including slant-, zigzag- and helical-shaped elements can be fabricated [6-11]. These nanostructured thin films have unique mechanical behaviors due to their characteristic nanoelements [12-16]. Thin films consisting of nanosprings have attracted considerable attention for various mechanical applications because they enable an extremely large elastic strain, which is very difficult to be achieved in solid films [17].

Electrical devices such as large-scale integrated circuits and nano/micro electromechanical systems contain large numbers of dissimilar interfaces because they are manufactured by the lamination of thin films. When the electronic device under loading or the surrounding temperature changed, the stress concentrate will appear near the free edge of interface, which could induce crack initiation at this point will bring about fatal malfunction of the device. Therefore, fracture often occurs in these devices at the electrical bonding interfaces between the dissimilar metallic materials. According to previous work, by inserting such a thin film between dissimilar components, the stress

singularity near the interface edge can be eliminated because of the low lateral stiffness of the nanospring thin film [18, 19]. Although fracture can be prevented by the insertion of a thin film of nanosprings at the interface as the characteristic mechanical properties eliminate the stress concentration, high electrical conductivity is required across the inserted thin film. Such a thermal interface element fabricated with GLAD copper (Cu) square spirals has recently been demonstrated [20].

In GLAD technique, nanosprings are grown on a substrate with atomic-scale shadowing (self-shadowing) and limited adatom diffusion [3, 4, 21], which prevents the vapor flux from reaching the regions behind evaporated nuclei. However, for low melting temperatures such as Cu [22] and Al [23], self-shadowing effect does not function effectively during the deposition because of their high adatom diffusion. According previous works [24, 25], although there have been previous reports of Cu and Al nanowhiskers formed on planar morphologies at elevated temperatures, the shape and the array structure of these nanowhiskers were uncontrollable, which emphasizes the difficulty of controlling the three-dimensional shapes of arranged nanoelements for metals with low melting temperature. Thus, to produce nanosprings of Cu and Al metals, it may be effective to hold the substrate at a low temperature to suppress surface diffusion. Although some Cu [26, 27] and Al [28] nanoelements have been produced by GLAD technique, there has no studies about the conditions for control of nanoshapes at low temperature.

Hence, in this chapter, a device was developed to control the temperature during GLAD and prepare a film consisting of Cu and Al nanoelements with controlled helical shapes. The substrate temperature for controlling the nanoshapes in the thin films was then investigated.

2.2 Experimental procedure

Figure 1(a) shows a schematic of the deposition apparatus, which consists of a vacuum evacuation system [turbomolecular pump (exhaust rate: 1000l/min) and rotary pump (exhaust rate: 90l/min)], a vapor evaporation system [vacuum chamber (inside diameter: 250 mm, base pressure: $< 5\times10^{-5}$ Pa), an electron beam (EB) evaporator (supply power: 3 kV), a manipulator with a rotation stage, and a quartz-type thickness meter], a temperature control system {stainless pipe for liquid nitrogen (LN_2) flow, a heater installed in the stage, a rod-shaped movable thermocouple [Type-K (chromel / alumel)]}, and a control apparatus. The distance between the evaporation source and the centerline of the substrate was 400 mm. Figure1 (b) shows the detailed configuration of the rotation stage, which consists of a Cu disk-shape substrate holder (60 mm diameter, 6 mm thick) mounted on an Inconel stage and a phosphor bronze ribbon. The phosphor bronze ribbon, of which the ends are joined to the outside surface of the stainless pipe, is in direct contact with the side surface of the stage. During GLAD, the stage is rotated in the in-plane direction while it maintains contact with the phosphor bronze ribbon. The LN_2 flowing in the stainless pipe decreases the substrate temperature through the stage and the phosphor bronze ribbon. The substrate temperature is controlled by the heater installed in the stage under a fixed LN_2 flow rate.

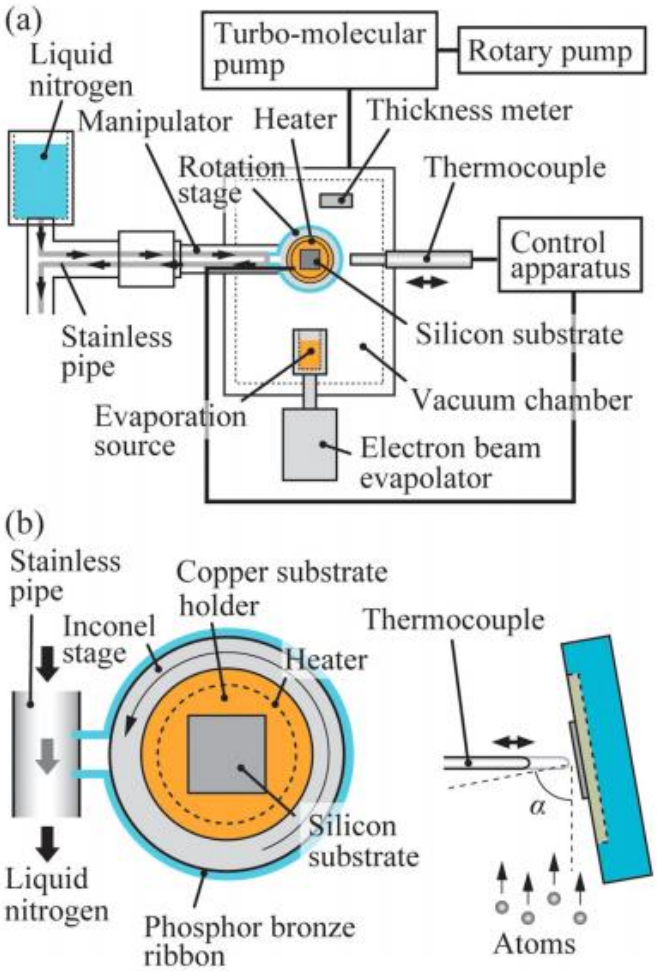

FIG. 1. (a) Schematic illustration of the deposition apparatus including the substrate temperature control system, and (b) detailed configuration of the rotation stage at the end of the manipulator.

A double-faced, highly polished square silicon (Si) (100) ($2\times2cm^2$, $550\mu m$ thick) is tightly attached to the Cu substrate holder with Kapton tape. The substrate temperature T_s is measured with the movable thermocouple, which is arranged at a location facing the substrate surface and is in contact with the center of the substrate under a constant pressure. The thermocouple was calibrated and preliminary measurements confirmed that the variance of the temperature distribution on the substrate was within 1% under similar conditions using thin film thermocouples directly attached to the substrate surface. When the substrate temperature was confirmed to be stable for more than 30 min after reaching the target temperature, GLAD was performed within 10s after removal of the thermocouple. The substrate temperature was measured again by bringing the thermocouple into contact with the substrate within 10 s after completion of the GLAD process. The difference between the temperatures measured before and after deposition was ± 1.5 °C. The thermal capacity of the Cu substrate holder is one hundred times or more greater than that of the Si substrate; therefore, the heat produced on the thin substrate during deposition was immediately absorbed by the Cu holder. In this work, the average value of the temperatures measured before and after deposition was defined as the representative substrate temperature, T_s.

GLAD was performed using the EB evaporator at 1.0×10^{-3} Pa on a Si substrate with a native oxide layer (SiO_2). The incidence angle α, defined as the angle between the incident flux and the substrate normal, is set to 84°. The angular accuracy of the tilting stage was 0.1°. Cu thin films were deposited at T_s = 453, 353, 323, 300, and 253 K, while the substrate was rotated so that *n*, the number of turns in each helix, was 4. Al thin films were formed at T_s = 300,253, and 233 K with n = 3. The substrate was rotated in the in-plane direction at a rate of 0.1 rpm. The deposition rate, which was monitored with a

thickness meter, was 5 Å/s. All thin films produced were observed using field-emission scanning electron microscopy (FE-SEM; Hitachi High-Tech, S-5500) after deposition.

2.3 Results and discussion

To determine the growth of the nanosprings, we focused on the axis line that passes through the center of nanoelement. When the axis line possessed a periodic shape with the target number of turns (Cu: $n = 4$ and Al: $n = 3$), it was determined that nanosprings were successfully grown. Figures 2(a)-2(e) show cross-sectional FE-SEM images of Cu thin films. At $T_s = 453$, 353, and 323 K [Figs. 2(a)-2(c)], isolated nanoscale protrusions without a periodic axis line were formed on the substrate. Their shape was irregular, but almost symmetrical with respect to the longitudinal axis. Full-grown protrusions were sparse, but low (100-200 nm height) protrusions were observed among them. At $T_s = 300$ and 253 K, the axis lines of the nanostructures had a periodic shape with $n = 4$, which indicated that helices were successfully grown. Therefore, the critical temperature to produce Cu nanosprings was between $T_s = 300$ and 323 K.

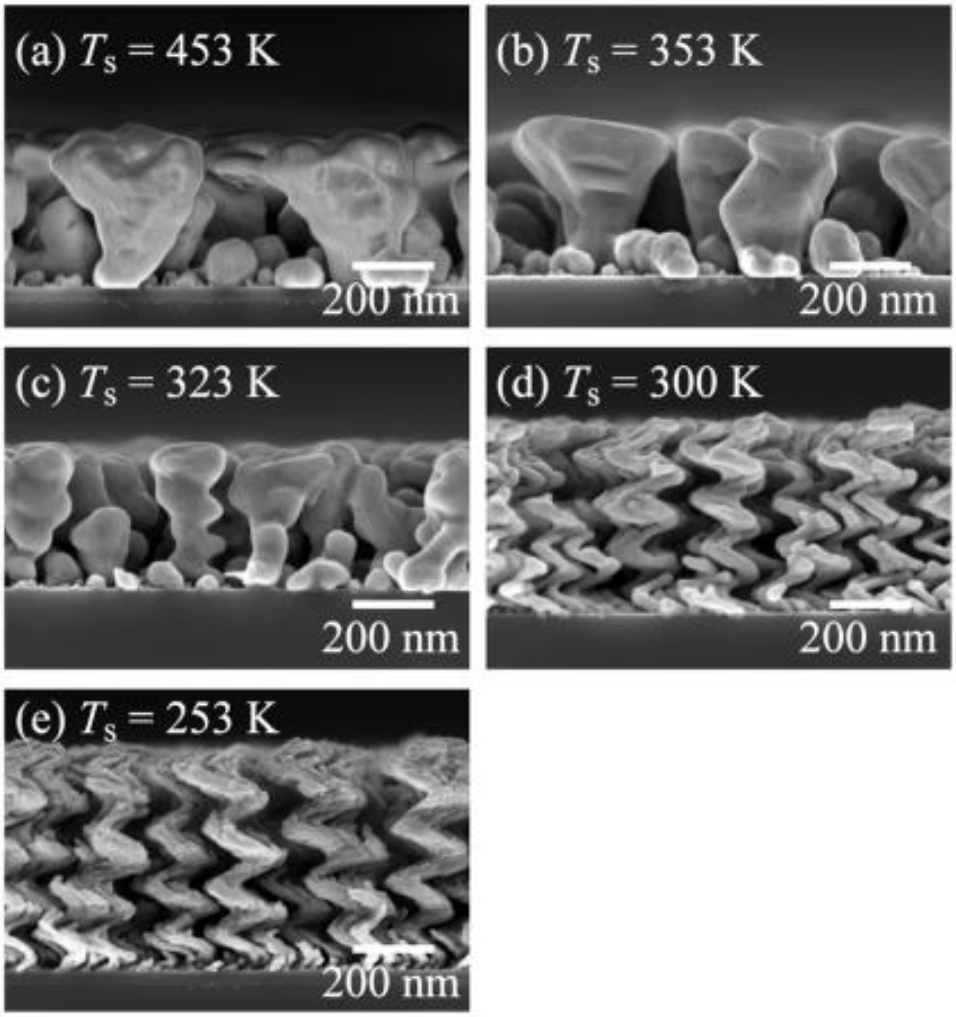

FIG. 2. FE-SEM images of Cu nanostructure arrays deposited at substrate temperatures of (a) 453, (b) 353, (c) 323, (d) 300, and (e) 253 K.

Figure 3 shows the average heights $\bar{h}$, the outer diameter at a height of 200 nm $\bar{D}_{200}$, the wire diameter at a height of 200 nm $\bar{d}_{200}$, the ratio of the wire diameter at a height of 300 nm to that at 100 nm $\bar{d}_{300}/\bar{d}_{100}$, and the angle of the coiled line axis with respect to the substrate normal, $\bar{\theta}$. $\bar{h}$ and $\bar{\theta}$ decreased while $\bar{D}$ and $\bar{d}_{300}/\bar{d}_{100}$ increased with increasing substrate temperature.

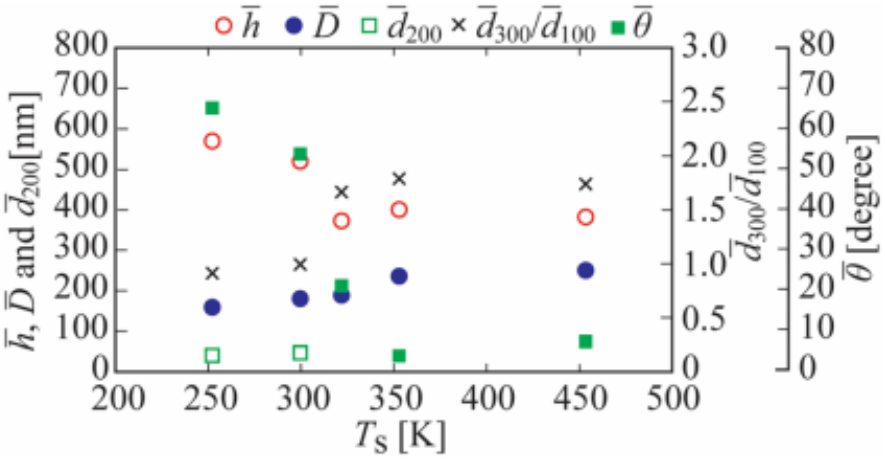

FIG. 3. Dependence of feature dimensions for Cu nanoelements on substrate temperature

To provide further information on the understructure, the nanosprings were examined by x-ray diffraction (XRD) analysis with achromatic Cu K_α radiation (λ = 1.542 Å), and the results are shown in Fig.4. The thin film of Cu nanosprings produced at T_s = 300 K have strong (111), (200), (220), and (311) textures normal to the surface. The grain size d_g was calculated as 27 nm using Scherrer's formula [29] [$d_g = 0.9\lambda/(\beta\cos\theta)$], where β is the full width at half maximum of the diffraction peak and θ is the diffraction angle.

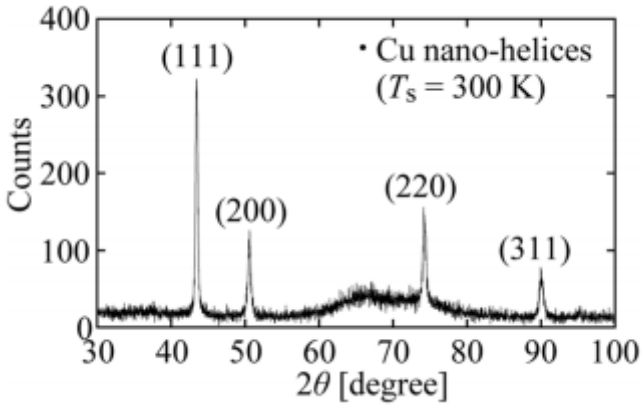

FIG. 4. XRD pattern for thin film of Cu nanosprings produced at T_s = 300 K.

Figures 5(a) - 5(c) show cross-sectional SEM images of Al nanostructures. At T_s = 300 K, the axis lines of the nanostructures did not have a periodic shape. Although the nanostructure was wavy at T_s = 253 K, no periodic shape could be identified. Al helices were successfully produced at T_s = 233 K; therefore, the critical temperature to produce a thin film of Al nanosprings was somewhere between T_s = 233 and 253 K.

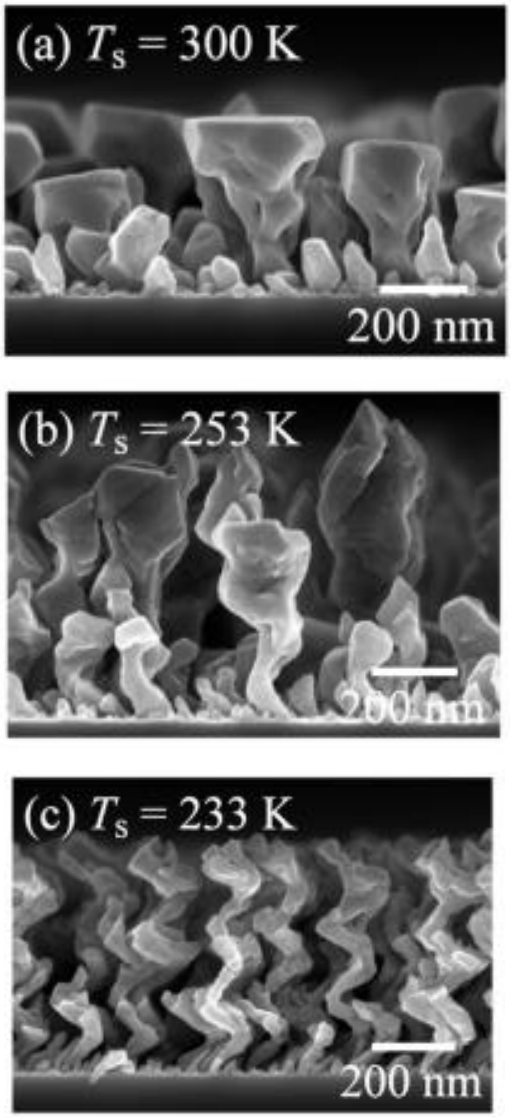

FIG. 5. Al nanostructure arrays deposited at substrate temperatures of (a) 300, (b) 253, and (c) 233 K.

Figure 6 shows $\bar{h}$, $\bar{D}_{200}$, $\bar{d}_{200}$, $\bar{d}_{300}/\bar{d}_{100}$, and $\bar{\theta}$ for Al nanoelements as a function of the substrate temperature. $\bar{h}$ and $\bar{\theta}$ decreased while $\bar{D}$ and $\bar{d}_{300}/\bar{d}_{100}$ increased with increasing the substrate temperature.

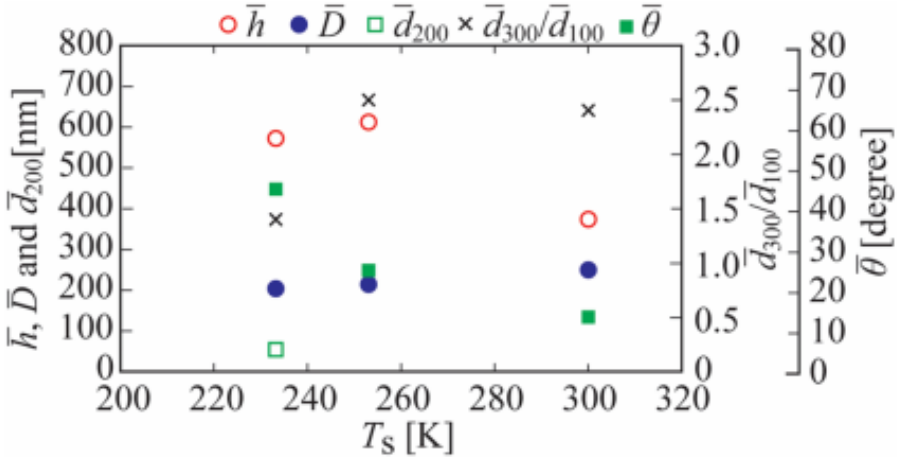

FIG. 6. Dependence of feature dimensions for Al nanoelements on substrate temperature.

Figure 7 shows an XRD pattern for the Al thin film produced at T_s = 233 K. Unlike Cu, only the (200) texture was observed. It has been reported that the orientation of crystallographic texture is strongly dependent on the material [30] and the deposition parameters (e.g., substrate surface conditions [31] and element shape [32]). Thus, a systematic study is required in future work to clarify the preferred texture of nanosprings produced by GLAD. The grain size d_g, calculated using Scherrer's formula, was 63 nm.

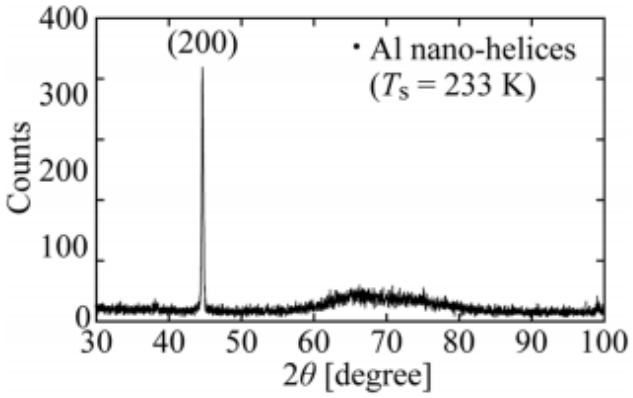

FIG. 7. XRD pattern for thin film of Al nanosprings produced at T_s = 233 K.

Figure 8 shows the dependence of the nanostructure shape on the substrate temperature T_s, normalized by the melting temperature of the target material, T_m. The results for nickel (Ni), which were obtained separately in another project, are also plotted for comparison. The critical temperatures to produce Cu, Al, and Ni nanosprings were T_s/T_m = 0.22–0.24, 0.25–0.27, and 0.22–0.26, respectively (T_m = 1358 K for Cu, T_m = 933 K for Al, and T_m = 1728 K for Ni). These values correspond to the critical homologous temperature (T_s/T_m = 0.24 ± 0.02) [33] at which the morphology of the nanostructure changes from broad columns (protrusions) to rods with high aspect ratios during GLAD for materials with melting temperatures above 1500 K (such as tantalum[34–36], niobium [37], chromium[36], and silicon[38, 39]). It should be noted that this is different from the critical homologous temperature Θ (= T_s/T_m) [40], which corresponds to a transformation from a nanocolumn (nanoprotrusion) to a planar morphology.

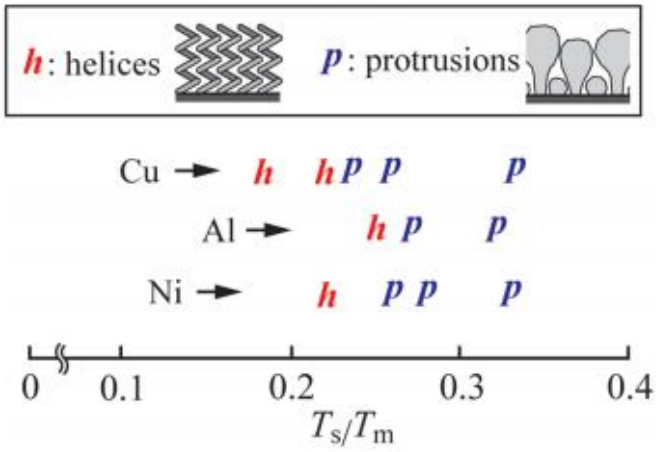

FIG. 8. Nanostructures formed by GLAD as a function of T_s/T_m.

A structure zone model (SZM) has been proposed for solid films grown under typical conditions where the flux is normal to the substrate surface [41]. In the SZM, the microstructures of films are classified into three distinct structural zones (zones I, II, and III), independent of the material, as a function of the homologous temperature T_s/T_m. In zone I ($T_s/T_m \leq 0.2$), low adatom mobility leads to narrow columnar structures characterized by ballistic growth, which results in a film containing voids between fibroid columns. In zone II ($0.3 \leq T_s/T_m \leq 0.5$), a polycrystalline structure appears in the evaporated film because adatoms actively fill the voids between nuclei through surface diffusion. In zone III ($0.5 \leq T_s/T_m$), bulk diffusion is dominant and causes recrystallization as the film grows. The critical temperature obtained in this work corresponds fairly well with the boundary between zones I and II in the SZM model, where surface diffusion becomes active. Thus, for $T_s/T_m < 0.22$, diffusion was sufficiently suppressed to maintain the shape of the nanoelements, which enabled the successful production of Cu and Al nanosprings using GLAD.

2.4 Conclusions

In this chapter, a developed GLAD system successfully produced Cu and Al nanosprings by maintaining the substrate temperature at $T_s/T_m < 0.22$, which corresponds to the transitional homologous temperature between zones I and II in the SZM for a solid film. This indicates that the formation of Cu and Al nanosprings is dependent upon the surface diffusion activity. XRD analysis indicated that the Cu and Al nanosprings were composed of coarse oriented grains with high crystallinity.

References in chapter 2

[1] Robbie, Kevin, Michael J. Brett, and Akhlesh Lakhtakia. "First thin film realization of a helicoidal bianisotropic medium." Journal of Vacuum Science & Technology A 13.6 (1995): 2991-2993.

[2] Robbie, Kevin, Michael J. Brett, and Akhlesh Lakhtakia. "Chiral sculptured thin-films." Nature 384.6610 (1996): 616-616.

[3] Robbie, Kevin, and M. J. Brett. "Sculptured thin films and glancing angle deposition: Growth mechanics and applications." Journal of Vacuum Science & Technology A 15.3 (1997): 1460-1465.

[4] Messier, Russell, Vijayakumar C. Venugopal, and Paul D. Sunal. "Origin and evolution of sculptured thin films." Journal of Vacuum Science & Technology A 18.4 (2000): 1538-1545.

[5] Hawkeye, Matthew M., and Michael J. Brett. "Glancing angle deposition: fabrication, properties, and applications of micro-and nanostructured thin films." Journal of Vacuum Science & Technology A 25.5 (2007): 1317-1335.

[6] Li B, Luo Z, Ho P S, et al. "Nanoindentation Study of the Mechanical Behavior of Silicon Nano-springs." AIP Conference Proceedings. IOP INSTITUTE OF PHYSICS PUBLISHING LTD, 2003: 525-532.

[7] Potocnik, J., Nenadovic, M., Jokic, B., Popovic, M., and Rakocevic, Z. (2016). "Properties of Zig-Zag Nickel Nanostructures Obtained by GLAD Technique."

Science of Sintering, 48(1), 51.

[8] Wang, Sumei, et al. "Structural and optical properties of nanostructured TiO 2 thin films fabricated by glancing angle deposition." Journal of alloys and compounds 431.1 (2007): 287-291.

[9] Lintymer, J., et al. "Glancing angle deposition to modify microstructure and properties of sputter deposited chromium thin films." Surface and Coatings Technology 174 (2003): 316-323.

[10] Kesapragada, S. V., and D. Gall. "Anisotropic broadening of Cu nanorods during glancing angle deposition." Applied physics letters 89.20 (2006): 203121.

[11] C.M. Zhou, D. Gall, "The structure of Ta nanopillars grown by glancing angle deposition." Thin Solid Films 515 (2006) 1223-1227.

[12] Kesapragada, S. V., et al. "Nanospring pressure sensors grown by glancing angle deposition." Nano letters 6.4 (2006): 854-857.

[13] A. Lakhtakia, Mater. Sci. Eng., C, Biomim. Mater., Sens. Syst. 19 (2002) 427.

[14] Singh J P, Karabacak T, Ye D X, et al. "Physical properties of nanostructures grown by oblique angle deposition." Journal of Vacuum Science & Technology B, 2005, 23(5): 2114-2121.

[15] Dick, B., et al. "Periodic magnetic microstructures by glancing angle deposition." Journal of Vacuum Science & Technology A 18.4 (2000): 1838-1844.

[16] H. Alouach, H. Fujiwara, G.J. Mankey, J. Vac. Sci. Technol., A 23 (2001) 1046.

[17] Sumigawa, Takashi, et al. "Effect of interface layer consisting of nanosprings on

stress field near interface edge." Engineering Fracture Mechanics 76.9 (2009): 1336-1344.

[18] Sumigawa, Takashi, et al. "Disappearance of stress singularity at interface edge due to nanostructured thin film." Engineering Fracture Mechanics 75.10 (2008): 3073-3083.

[19] Sueda, Taisuke, et al. "Stress singularity transition of generic wedges due to nanoelement layers." Engineering Fracture Mechanics 78.16 (2011): 2789-2799.

[20] D. Shaddock, S. Weaver, I. Chasiotis, B. Shah, and D. Zhong, Proceedings of the ASME 2011 Pacific Rim Technical Conference and Exposition on Packaging and Integration of Electronic and Photonic Systems, MEMS and NEMS(ASME, Portland, OR, 2011), Vol. 2, p. 13.

[21] Krug, Joachim. "Origins of scale invariance in growth processes." Advances in Physics 46.2 (1997): 139-282.

[22] Harris, K. D., Sit, J. C., and Brett, M. J. "Fabrication and optical characterization of template-constructed thin films with chiral nanostructure." IEEE transactions on nanotechnology, 1.3 (2002), 122-128.

[23] Dick, B., Brett, M. J., and Smy, T. "Controlled growth of periodic pillars by glancing angle deposition." Journal of Vacuum Science & Technology B, 21.1(2003), 23-28.

[24] Suzuki, M., Nagai, K., Kinoshita, S., Nakajima, K., Kimura, K., Okano, T., and Sasakawa, K.. "Vapor phase growth of Al whiskers induced by glancing angle deposition at high temperature." Applied physics letters, 89.13 (2006), 133103.

[25] Mukherjee, S., Zhou, C. M., and Gall, D. "Temperature-induced chaos during nanorod growth by physical vapor deposition." Journal of Applied Physics, 105.9 (2009), 094318.

[26] Karabacak, T., G-C. Wang, and T-M. Lu. "Physical self-assembly and the nucleation of three-dimensional nanostructures by oblique angle deposition." Journal of Vacuum Science & Technology A 22.4 (2004): 1778-1784.

[27] Karabacak, Tansel, et al. "Low temperature melting of copper nanorod arrays." Journal of applied physics 99.6 (2006): 064304.

[28] Jen, Yi-Jun, and Ching-Wei Yu. "Metal and dielectric duality for an aligned Al nanorod array." Applied physics letters 91.2 (2007): 021109.

[29] B. E. Warren, X-ray Diffraction (Dover, New York, 1990).

[30] LaForge, Joshua M., et al. "Flux engineering to control in-plane crystal and morphological orientation." Crystal Growth & Design 12.7 (2012): 3661-3667.

[31] Alouach, H., and G. J. Mankey. "Texture orientation of glancing angle deposited copper nanowire arrays." Journal of Vacuum Science & Technology A 22.4 (2004): 1379-1382.

[32] Chen, Liang, et al. "Engineering epitaxial-nanospiral metal films using dynamic oblique angle deposition." Crystal Growth & Design 13.5 (2013): 2075-2080.

[33] Mukherjee, S., and D. Gall. "Structure zone model for extreme shadowing conditions." Thin Solid Films 527 (2013): 158-163.

[34] Zhou, C. M., and D. Gall. "Competitive growth of Ta nanopillars during glancing

angle deposition: Effect of surface diffusion." Journal of vacuum science & technology. A. Vacuum, surfaces, and films 25.2 (2007): 312.

[35] Zhou, C. M., and D. Gall. "Growth competition during glancing angle deposition of nanorod honeycomb arrays." Applied Physics Letters 90.9 (2007): 93103-93103.

[36] Mukherjee, S., and D. Gall. "Power law scaling during physical vapor deposition under extreme shadowing conditions." Journal of Applied Physics 107.8 (2010): 084301.

[37] Mukherjee, S., and D. Gall. "Anomalous scaling during glancing angle deposition." Applied Physics Letters 95.17 (2009): 173106.

[38] Karabacak, T., et al. "Scaling during shadowing growth of isolated nanocolumns." Physical Review B 68.12 (2003): 125408.

[39] Patzig, Christian, and Bernd Rauschenbach. "Temperature effect on the glancing angle deposition of Si sculptured thin films." Journal of Vacuum Science & Technology A 26.4 (2008): 881-886.

[40] Deniz, Derya, and Robert J. Lad. "Temperature threshold for nanorod structuring of metal and oxide films grown by glancing angle deposition." Journal of Vacuum Science & Technology A 29.1 (2011): 011020.

[41] Movchan, B. A., and A. V. Demchishin. "STRUCTURE AND PROPERTIES OF THICK CONDENSATES OF NICKEL, TITANIUM, TUNGSTEN, ALUMINUM OXIDES, AND ZIRCONIUM DIOXIDE IN VACUUM." Fiz. Metal. Metalloved. 28: 653-60 (Oct 1969). (1969).

Chapter 3 Elastic limit of a thin film consisted of nickel nanosprings

3.1 Introduction

By inserting the nanospring thin film [1-10] at the interface between dissimilar materials, the stress concentration at the interface is eliminated, and thus interface delamination is successfully prevented within the multi-layered electronic devices [11-15]. For the potential application in advanced electronic devices, beside the electrical conductivity, the yielding behavior of nanospring thin films which might induce the fetal malfunction of electronic devices should be also carefully considered.

The shape and size of nanoelement could strongly influence the mechanical properties of thin film [5, 6]. For example, as tall helical nanoelement has different vertical and lateral stiffness, a thin film comprising of them shows strong characteristic anisotropy [14, 15]. Moreover, the anisotropy can be controlled by the height of nanoelement. As the stiffness of element is depending on the shape (slant bar, zigzag and spring), the apparent elastic modulus of film is also controllable [16, 17]. It is well known that helical shape can sustain large reversible deformation. Thus we expect a thin film composed of helical nanoelements (nanospring thin film) may has giant elastic limit. For the design of microelectronic devices, the engineer pay attention to the yielding behavior of metals. Although, there are many research work focus on the mechanical properties of GLAD thin film [6, 8, 9, 11, 14], there has been no work on the yield behavior of nanosprings

film.

Thus, in this chapter, a thin film composed of nickel nanosprings is fabricated, and its elastic limit are characterized by loading tests using an atomic force microscope (AFM). Then, based on the experimental results, we numerically analyzed the stress distribution in nanospring by finite element method (FEM).

3.2 Experiment procedures

3.2.1 Tested material

Figure 1(a) shows the process of forming a nanosprings film using the GLAD technique. The atoms are deposited on the substrate with an oblique angle α (the angle between the incident direction and the normal of the substrate) and these make numerous islands at the early stage of deposition. Once islands are formed, successive atoms cannot reach the other side by the oblique deposition (shadow effect). Thus, each island grows in one direction and forms a slanted nano-bar. As the substrate rotates during the deposition, the growth direction is twisted, and this results in bars with helical shape [1-6].

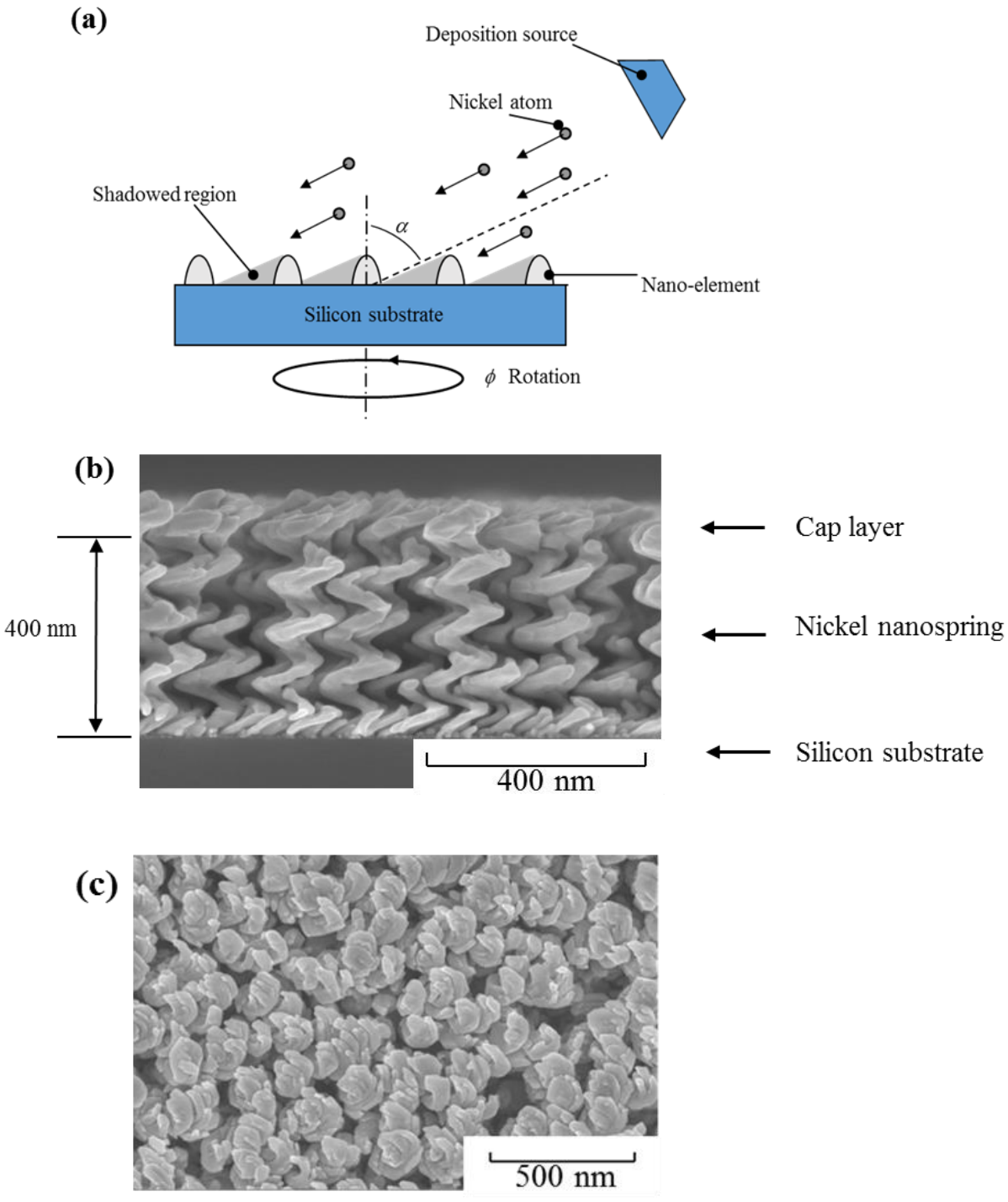

Fig. 1. (a) Schematic depiction of nanospring thin film growth by glancing angle deposition (GLAD) technique. (b) Cross-sectional SEM images of thin film that consist of Nickel helical nanospring and (c) Top-view SEM image.

The material investigated here is a thin film of nickel nanosprings formed on a 525-μm-thick silicon (100) substrate by the deposition using electron-beam evaporation with an oblique angle α of 86° under vacuum (1.0×10^{-3} Pa). In order to apply the load, the cap layer is deposited on the top of nanosprings as shown in Fig. 1b. The rotation speed of the substrate is 0.4 deg/s. Table 1 shows the average size of nanospring measured by a scanning electron microscope (SEM).

Table 1 Dimensions of a single nickel nanospring.

n	h_s (nm)	d (nm)	R (nm)	L (nm)
4	400	25	62.5	135

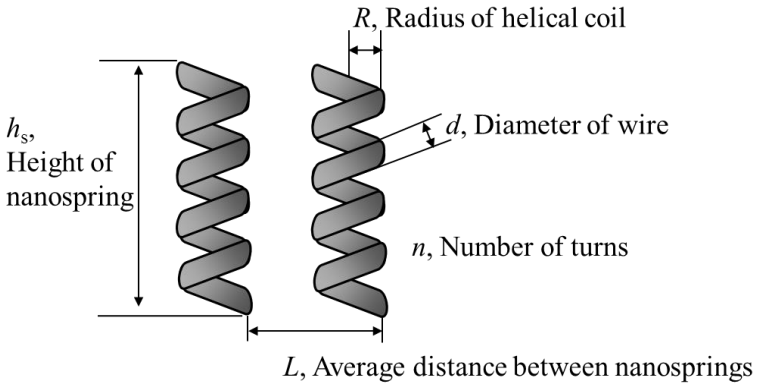

3.2.2 Loading method

A compression load, F_v, is applied to the nanosprings film using an atomic force microscope (AFM) [18] with a loading apparatus (Hysitron: Tribosocope) that can precisely measure the vertical displacement of the loading tip δ_v during compression as shown in Fig. 2. Additionally, by observing the AFM image of the specimen, we can apply the load at the desired position. The curvature of hemispherical diamond tip is approximately 10.44 μm which is much larger than the nanosprings and their spaces as shown in Fig. 2. The loading rate dF_v/dt is 5 μN/s.

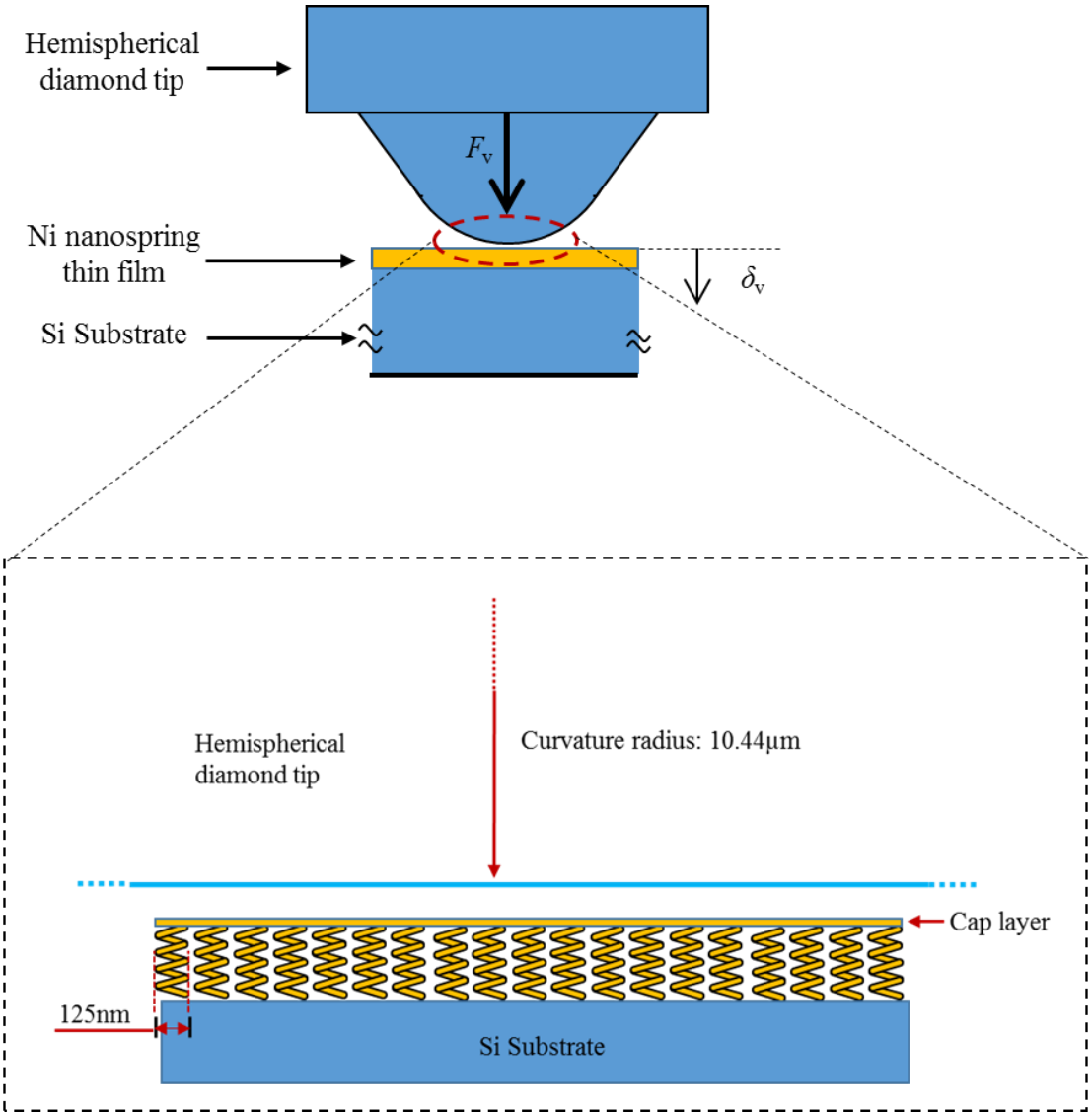

Fig. 2. Illustration of the loading method by the atomic force microscope (AFM) with a hemispherical tip and the magnified picture of loading area.

3.3 Results and Discussion

3.3.1 Elastic limit

Figure 3 shows load-displacement curves under compression. After the applied load reaches F_v = 19.0 μN (δ_v = 19.2 nm), the nanospring is unloaded. There is no difference between the loading and unloading curves, which indicates fully "elastic" deformation. Then, same load (F_v = 19.0 μN) is applied at the same position in order to confirm the reversible deformation. As the second loading and unloading curves are almost the same as the first, as shown in Fig. 3 (a), there is no inelastic (plastic) deformation. In a similar way, Figure 3(b) clarifies that no inelastic deformation appears in the loading up to F_v = 20.2 μN (δ_v = 20.9 nm). However, when the load reaches 21.9 μN (δ_v = 21.7 nm), the second loading curve is different from the first, as shown in Fig. 3(c). This indicates that a residual displacement remains after the first loading. In other words, the nanopsrings undergo inelastic deformation. However, as the inelastic deformation is small, it is not clear in the load-displacement curves. Therefore, we apply a higher load of 23.0 μN in order to identify the appearance of plasticity. As shown in Fig. 3(d), the remaining displacement reaches 5 nm after fully unloading (F_v = 0 μN). This demonstrates that the nanosprings yield somewhere between δ_v = 20.9 nm (F_v = 20.2 μN) and δ_v = 21.7 nm (F_v = 21.9 μN).

We conduct compression test three times at different locations on the thin film, and Table 2 lists the yield displacement and relevant apparent yield strain ε'_Y. For various loading, the yield displacement $\delta_{v,Y}$ has little fluctuation around 22.7 ± 1.9 nm, which indicates that yield displacement is an intrinsic property for the nickel nanosprings film.

The apparent yield strain of nanosprings film ε'_Y is given by:

$$\varepsilon'_{\mathrm{Y}} = \frac{\delta_{\mathrm{v,Y}}}{h_s} \quad (1)$$

where h_s is height of nanospring. As the film yields at $\delta'_{\mathrm{v,Y}}$ = 20.8 ~ 24.6 nm, the apparent yield strain is 5.2 ~ 6.15×10^{-2}, as listed in Table 2. Since the yield strain of a bulk Ni is ε_{Y} = 2.9 ~ 4.4×10^{-4} [19], nanosprings film has about 200 times larger one. This means that the Ni nanosprings film has giant elastic limit than the bulk counterpart.

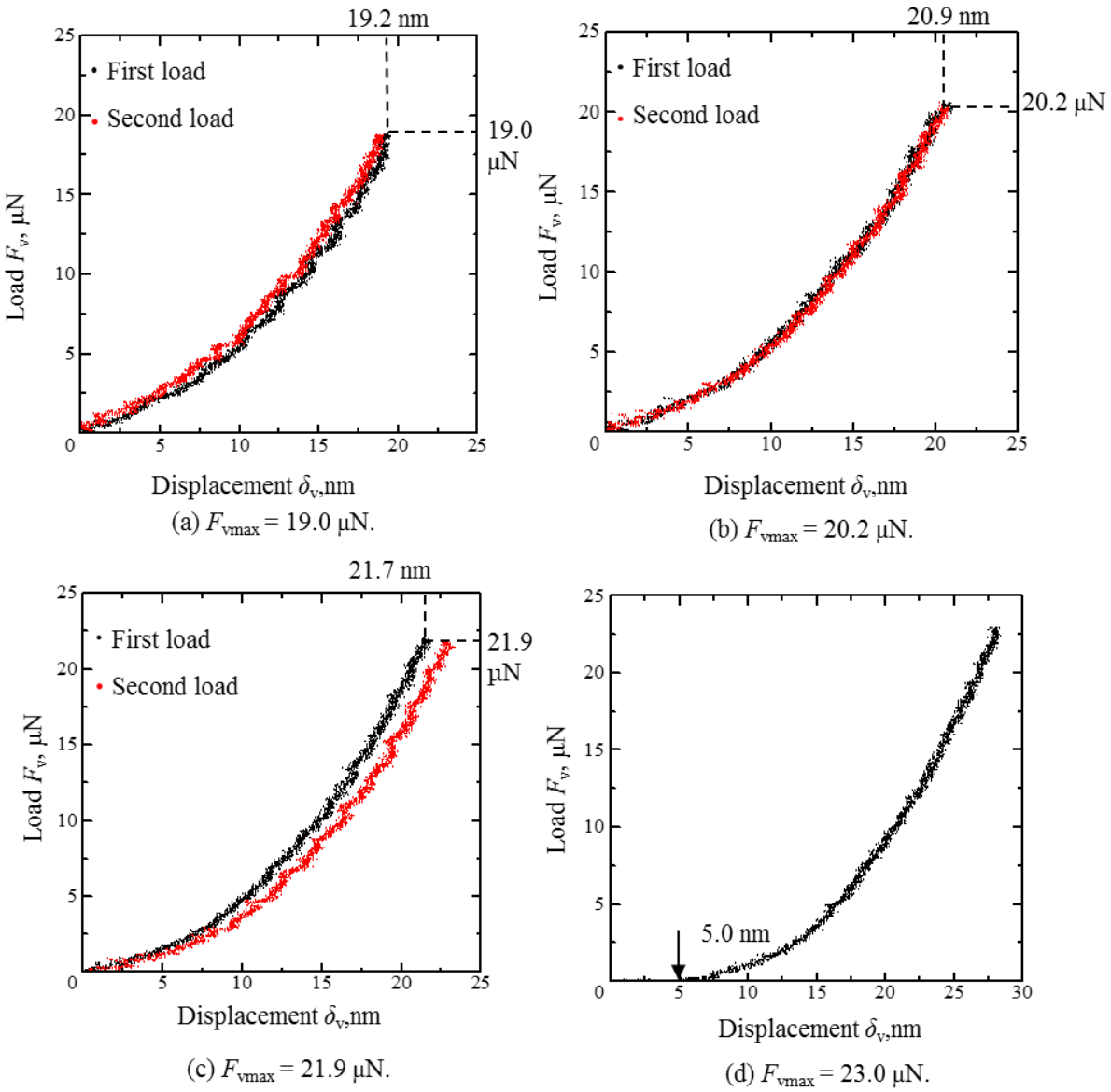

Fig. 3. The load versus displacement curves of compression test in location 1 with various maximum loading values.

Table 2 Yield displacement and apparent yield strain of 3 locations.

Location No.	$\delta_{V,Y}$, **nm**	ε'_Y
1	21.7	5.4×10^{-2}
2	24.6	6.15×10^{-2}
3	20.8	5.2×10^{-2}

3.3.2 Effect of helical shape

In order to extract the effect of helical shape on the apparent yield strain, we conduct an approximate analysis on the spring and a bulk with a same mechanical behavior such as the elastic constants and the yield stress.

The vertical displacement δ_{spring} of a loading spring roughly has the following relationship [20]:

$$\delta_{\text{spring}} = \frac{64nWR^3}{d^4G} \tag{2}$$

where *W*, *G*, *n*, *R* and d are denoted as the loading value, the shear modulus, the number of turns, the radius of the spring and the diameter of the wire, respectively. The maximum shear stress on the wire is given by [20]:

$$\tau_{\max} = \frac{16WR}{\pi d^3} \tag{3}$$

Combing Eq. (2) and (3) and assuming the Tresca yield criterion, τ_{Y}, for simplicity, the yield apparent strain $\varepsilon'_{\text{spring}}$ of spring has the form,

$$\varepsilon'_{\text{sping,Y}} = \frac{4\pi nR^2\tau_{\text{Y}}}{Gh_{\text{s}}d} \tag{4}$$

where h_{s} is the spring height. On the other hand, the yield strain of solid film under uniaxial tension is given by

$$\varepsilon_{\text{solid,Y}} = \frac{\sigma_{\text{Y}}}{E} = \frac{2\tau_{\text{Y}}}{E} \tag{5}$$

Thus, the ratio γ of $\varepsilon'_{\text{spring,Y}}$ to $\varepsilon_{\text{solid,Y}}$ can be estimated using the following expression:

$$\gamma = \frac{\varepsilon'_{\text{spring,Y}}}{\varepsilon_{\text{solid,Y}}} = \frac{2\pi nR^2E}{Gh_{\text{s}}d} \tag{6}$$

By inserting $G = E/\{2(1+\nu)\}$, $n = 4$, $R = 62.5$ nm, $E = 200$ GPa, $h_{\text{s}} = 400$ nm, $d = 25$ nm and $\nu = 0.31$ into Eq. (6), we obtain $\gamma \approx 25$. This means that the helical shape increases the yield strain by approximately 20 times because the torsional shear stress is dominant

in the spring wire. As this is much smaller than the experimental result shown in section 3.1 (200 times), the giant elastic limit of nanospring film cannot be explained by only the shape effect of nanoelements.

3.3.3 Size effect of element

It is well known that the yield stress (yield strain) of a nanometer-scale metal is remarkably higher than that of the bulk [21, 22]. The main causes are the understructure of materials; fine grains [23, 24], higher density of vacancies [25], starvation of dislocation source [26] and so on. Thus, we can suspect size effect (morphology of understructure) is another indispensable factor. The stress in a nanospring is analyzed using a three-dimensional finite element method (FEM) under linear elastic condition with Young's module of 200 GPa and Poisson's ratio of 0.31[19]. In the model, the shape and size of the nanospring are carefully reproduced depending on the average values obtained from the SEM images. Because the stress concentrates near the bottom due to the smaller diameter, the region is divided into fine meshes. Fixing the nodes at the bottom of nanospring, uniform distribution of compressive displacement, $\delta_{v,Y}$ = 22.7 nm, is applied to the nodes at the top of nanospring, as shown in Fig. 4(a). Here, as the load is applied to the spring through the cap layer as shown in Fig.1(c), the lateral displacement is restricted at the top of nanospring. Then, we apply the compressive displacement instead of the load.

Figure 4(b) shows the distribution of von Mises stress in the single nanospring model. The maximum stress appears at the internal surface of the first turn of the nanospring because it has thinnest wire diameter, and has a magnitude of about 1.2 GPa. Although this must bring about the yielding in the spring, it can not be experimentally observed because the localized plastic zone is very small. The magnitude of yield stress is approximately 20 times higher than that of bulk nickel, about 60 MPa [19].

On the other hand, it is suspected that the yield stress σ_Y and yield strain ε_Y of solid Ni thin film (with a thickness of 15 ~ 17 μm) [27] are approximately 10 times larger than

that of bulk Ni. This suggests that the size effect (morphological of understructure) increases the elastic limit for nanosprings film around 10 times. As it has been reported that the GLAD film usually has nano-sized grains, this might be attributed to the morphology. However, to examine the detail of understructure is beyond the target in this work and remains for future work.

It should be noted that the Ni nanosprings can absorb 200 times larger reversible (elastic) strain than the bulk Ni. Thinking the rough assumption in the analysis, the size effect provides the enhancement of approximately 10 ~ 20 times and the shape effect provides another 10 ~ 20 times. Designing the shape and size of elements, we can optimize the elastic limit. However, it remains for future work because the main purpose of this study is to show experimentally the existence of giant elastic limit caused by the nanosprings.

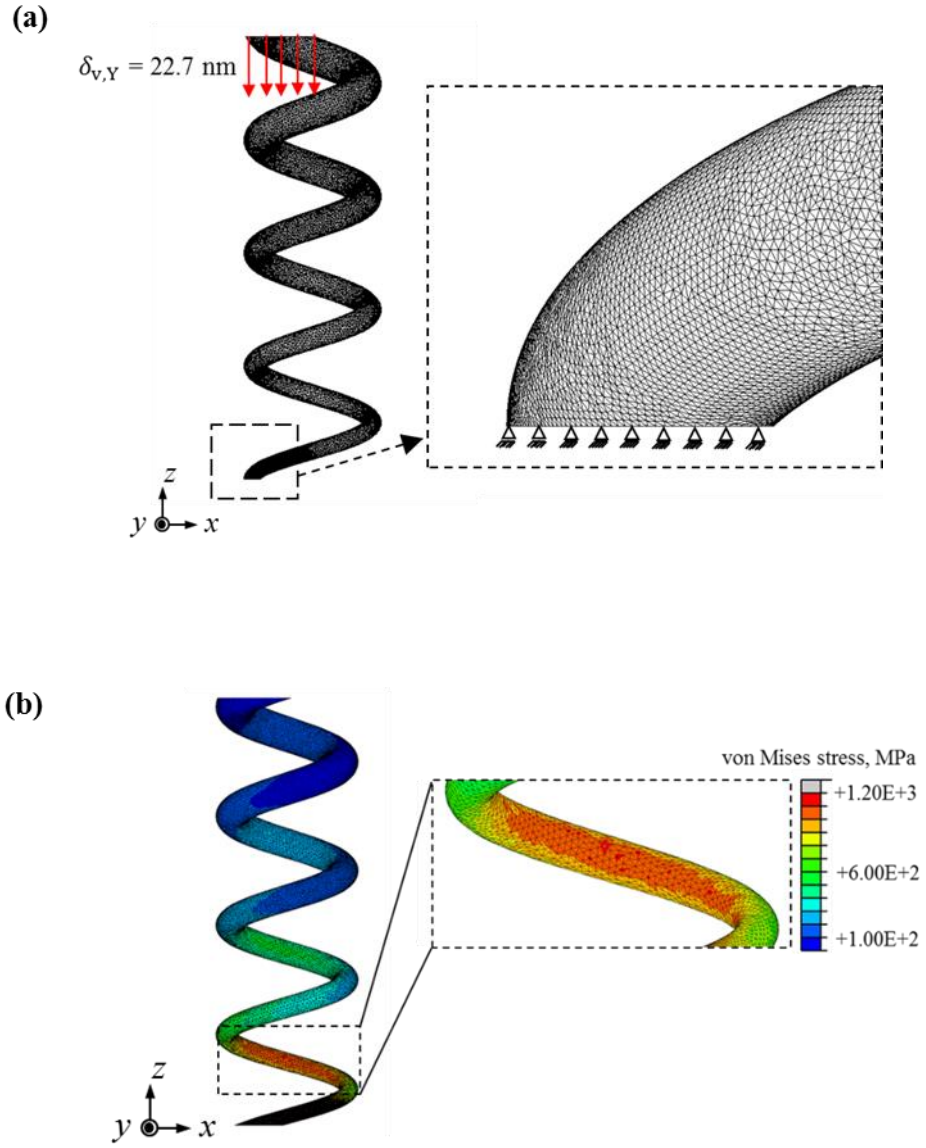

Fig. 4. The finite element model (FEM) of single nanospring: (a) The yield displacement ($\delta_{v,Y}$ = 22.7 nm) is applied at the top of FEM model. (b) The distribution of von Mises stress in single nanospring at the yield condition.

3.4 Conclusions

In this chapter, we investigated the elastic limit of a thin film comprising of Ni nanosprings fabricated by the GLAD technique applying compression by an AFM. The results are summarized as follow:

1. The Ni nanosprings thin film has giant elastic limit whose apparent yield strain is evaluated as $\varepsilon_Y' = 5.2 \sim 6.2\times10^{-2}$, which is almost 200 times larger than that of bulk Ni ($\varepsilon_Y = 0.29 \sim 0.44\times10^{-3}$).
2. The "shape effect (helical shape)" provides a high tolerance to the reversible deformation. In the material tested, the shape effect gives is around 10 ~ 20 times.
3. The "size effect (nano-sized element)" stem from the morphology of understructure leads to high yield stress (strain) for the springs, which enhances the relevant yield strain to the nanosprings film. The effect is a yield strain increase of approximately 10 ~ 20 times in the examined Ni nanosprings film.

References in Chapter 3

[1] Robbie, K., J. C. Sit, and M. J. Brett. "Advanced techniques for glancing angle deposition." Journal of Vacuum Science & Technology B 16.3 (1998): 1115-1122.

[2] Zhao, Y-P., et al. "Designing nanostructures for sensor applications." Journal of electronic materials 35.5 (2006): 846-851.

[3] Harris, Kenneth D., Jeremy C. Sit, and Michael J. Brett. "Fabrication and optical characterization of template-constructed thin films with chiral nanostructure." IEEE transactions on nanotechnology 1.3 (2002): 122-128.

[4] Steele, John J., and Michael J. Brett. "Nanostructure engineering in porous columnar thin films: recent advances." Journal of Materials Science: Materials in Electronics 18.4 (2007): 367-379.

[5] Seto, M. W., et al. "Mechanical response of thin films with helical microstructures." Journal of Vacuum Science & Technology B 17.5 (1999): 2172-2177.

[6] Seto, Mary W., Brian Dick, and Michael J. Brett. "Microsprings and microcantilevers: studies of mechanical response." Journal of Micromechanics and Microengineering 11.5 (2001): 582.

[7] Potocnik, J., Nenadovic, M., Jokic, B., Popovic, M., and Rakocevic, Z. (2016). "Properties of Zig-Zag Nickel Nanostructures Obtained by GLAD Technique." Science of Sintering, 48(1), 51.

[8] J. Lintymer, N. Martin, J.M. Chappe, P. Delobelle, J. Takadoum, "Influence of zigzag microstructure on mechanical and electrical properties of chromium multilayered thin films." Surf. Coat. Technol. 180-181 (2004) 26-32.

[9] S.V. Kesapragada, D. Gall, "Anisotropic broadening of Cu nanorods during glancing angle deposition." Appl. Phys. Lett. 89 (2006) article number: 203121.

[10] C.M. Zhou, D. Gall, "The structure of Ta nanopillars grown by glancing angle deposition." Thin Solid Films 515 (2006) 1223-1227.

[11] Li B, Luo Z, Ho P S, et al. "Nanoindentation Study of the Mechanical Behavior of Silicon Nano-springs." AIP Conference Proceedings. IOP INSTITUTE OF PHYSICS PUBLISHING LTD, 2003: 525-532.

[12] Sumigawa T, Sueda T, Futamura Y, et al. "Effect of interface layer consisting of nanosprings on stress field near interface edge." Engineering Fracture Mechanics. 2009, 76(9): 1336-1344.

[13] Sumigawa T, Hirakata H, Takemura M, et al. "Disappearance of stress singularity at interface edge due to nanostructured thin film." Engineering Fracture Mechanics. 2008, 75(10): 3073-3083.

[14] Hirakata H, Matsumoto S, Takemura M, et al. "Anisotropic deformation of thin films comprised of helical nanosprings." International journal of solids and structures, 2007, 44(11): 4030-4038.

[15] Hirakata H, Nishihira T, Yonezu A, et al. "Interface strength of structured nanocolumns grown by glancing angle deposition." Engineering Fracture Mechanics, 2011, 78(16): 2800-2808.

[16] Lintymer J, Martin N, Chappé J M, et al. "Nanoindentation of chromium zigzag thin films sputter deposited." Surface and Coatings Technology, 2005, 200(1): 269-272.

[17] Liu D L, Ye D X, Khan F, et al. "Mechanics of patterned helical Si springs on Si substrate." Journal of nanoscience and nanotechnology, 2003, 3(6): 492-495.

[18] Nagar, Rupali, et al. "Mechanical Characteristics of Silicon Nanostructures Using

Force Distance Spectroscopy." Journal of nanoscience and nanotechnology 10.5 (2010): 2994-3000.

[19] Metal Handbook, tenth ed., vol. 2, ASM International, (1990).

[20] A. M. Wahl, Mechanical Springs, second ed. McGraw-Hill, New York. (1963).

[21] Greer, Julia R., and William D. Nix. "Size dependence of mechanical properties of gold at the sub-micron scale." Applied Physics A 80.8 (2005): 1625-1629.

[22] Uchic, Michael D., et al. "Sample dimensions influence strength and crystal plasticity." Science 305.5686 (2004): 986-989.

[23] Hall, E. O. "The deformation and ageing of mild steel: III discussion of results." Proceedings of the Physical Society. Section B 64.9 (1951): 747.

[24] Cracknell, A., and N. J. Petch. "Frictional forces on dislocation arrays at the lower yield point in iron." Acta Metallurgica 3.2 (1955): 186-189.

[25] Sheng, Junjie, et al. "Dynamic electromechanical performance of viscoelastic dielectric elastomers." Journal of Applied Physics 114.13 (2013): 134101.

[26] Kumar, K. S., H. Van Swygenhoven, and S. Suresh. "Mechanical behavior of nanocrystalline metals and alloys." Acta Materialia 51.19 (2003): 5743-5774.

[27] H. Seungwoo, K. Taeok, L. Hakjoo and L. Hyunwoo, 2008 2nd Electronics System-Integration Technology Conference. (2008).

Chapter 4 *In situ* Observation of Tensile Behavior in a Single Silicon Nanospring

4.1 Introduction

Up to now, several methodologies have been developed to fabricate thin films consisting of discretely nano-sized sculptured elements [1-9]. Among these techniques, the glancing angle deposition (GLAD) method [10-25] is simple and efficient for forming the thin film of various shaped nano-elements on a substrate. In Chapter 3, the yield behavior of nanospring thin film has been investigated. However, the nanospring thin film is composed of numerous individual nanosprings, and each of them possesses non-uniform geometric shape. Therefore, to inquire the detailed information of deformation and fracture behaviors of nanospring thin films, mechanical properties of individual nanospring should be clearly clarified.

There have been a few previous studies to investigate the mechanical properties of GLAD films before [26-33]. However, it is usually measured by compression tests. In their studies, the combination of atomic force microscope (AFM) and nanoindentation is a common loading methods. In these tests, just the average magnitude is obtained since plural nanoelements are compressed at the same time. In actually, the thin film is composed of nano-element with slightly different shape. Furthermore, compression tests cannot offer the elongation at the fracture. Although there have been reports where the load is applied on an individual nanospring, these experiments are conducted under compression in the elastic region [32, 33]. If tensile test on an individual element is

conducted, the detailed mechanism involved in elasto-plastic deformation and fracture of each element can be determined. However, there have been no previous reports of such tests. In addition, although *in situ* observation using electron microscopy would provide details on the deformation and fracture processes for the element material, there is another difficulty to apply the load correctly under the high magnification observation.

In this chapter, a tensile testing method is developed for a single silicon nanospring prepared by the GLAD technique under *in situ* observation using scanning electron microscopy (SEM). Experiments are conducted for several springs to clarify the difference in the deformation and fracture properties among individual nanoelements extracted from the same film and elucidate the mechanism in detail.

4.2 Experimental procedure

4.2.1 Material and specimen

The thin film composed of silicon nanosprings is formed on a 525 μm thick Si(100) substrate using the GLAD technique. As an evaporant, high purity silicon (99.999 %) pieces (Nilaco corp.) are used. The crucible diameter is 30 mm. The distance between the evaporation source and the substrate is 400 mm. GLAD is performed under a vacuum of 1.0×10^{-3} Pa using electron-beam evaporation, where the deposition angle and rotation speed of the substrate are 86° and 0.3°/s, and 88° and 3.0°/s, respectively, for the nanospring and the upper nanobar. The evaporation rate is set around 10Å/s, which is controlled by a feedback system. The total time of deposition process is about 40 minutes. Figure 1 shows a cross-sectional image of the thin film composed of

nanosprings. A straight part (nanobar) is formed on the top of every nanospring for application of a tensile load. In this work, a loading tip is connected to a single nanoelement with an adhesive. In order to prevent the adhesive flow to the nanospring, the straight nanobar is established as a dummy part. Preliminary examination of electron diffraction patterns by means of a transmission electron microscope (TEM) clarifies that the GLAD film is an amorphous phase. Figure 2 shows the average size of nanoelements grown on the substrate, which is measured from SEM observation.

It should be noted that the spring wire diameter in the lower part of the nanospring is smaller than that in the upper part and there are numerous incomplete spring frameworks near the nanosprings on the substrate (See Fig. 1).

The deposited nanosprings are densely distributed; therefore, it is difficult to pick up a single nanospring for application of a precise tensile load. Hence, adjacent nanosprings around the target nanospring are removed, as shown in Fig. 3, using the nanoprobe device described in the next section. Three single nanospring specimens are prepared for tensile tests as shown in Fig. 4.

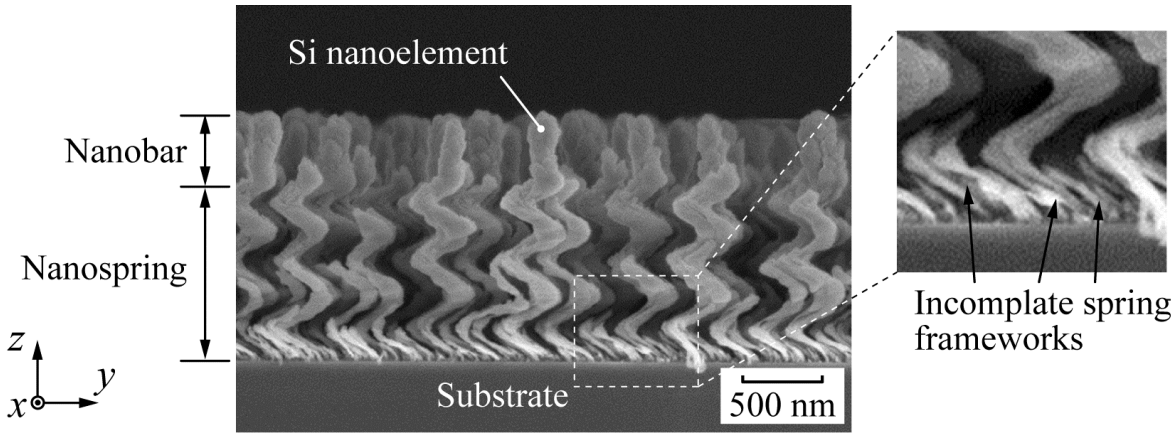

Fig. 1. Cross-sectional SEM image of thin film composed of silicon nanoelements.

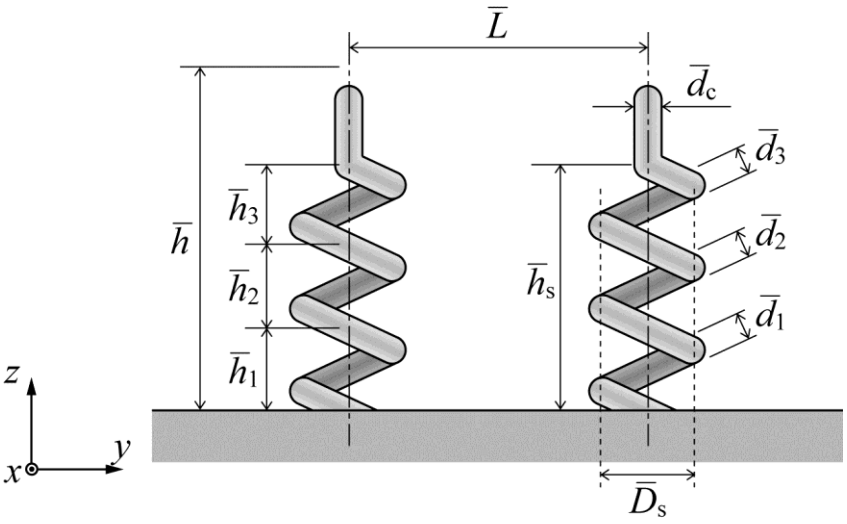

$\overline{h}$	$\overline{L}$	$\overline{d}_c$	$\overline{h}_s$	$\overline{D}_s$	$\overline{d}_1$	$\overline{d}_2$	$\overline{d}_3$	$\overline{h}_1$	$\overline{h}_2$	$\overline{h}_3$
1139	107	126	829	311	56	89	111	296	292	241

Fig. 2 Average dimensions of a nanospring (units: nm).

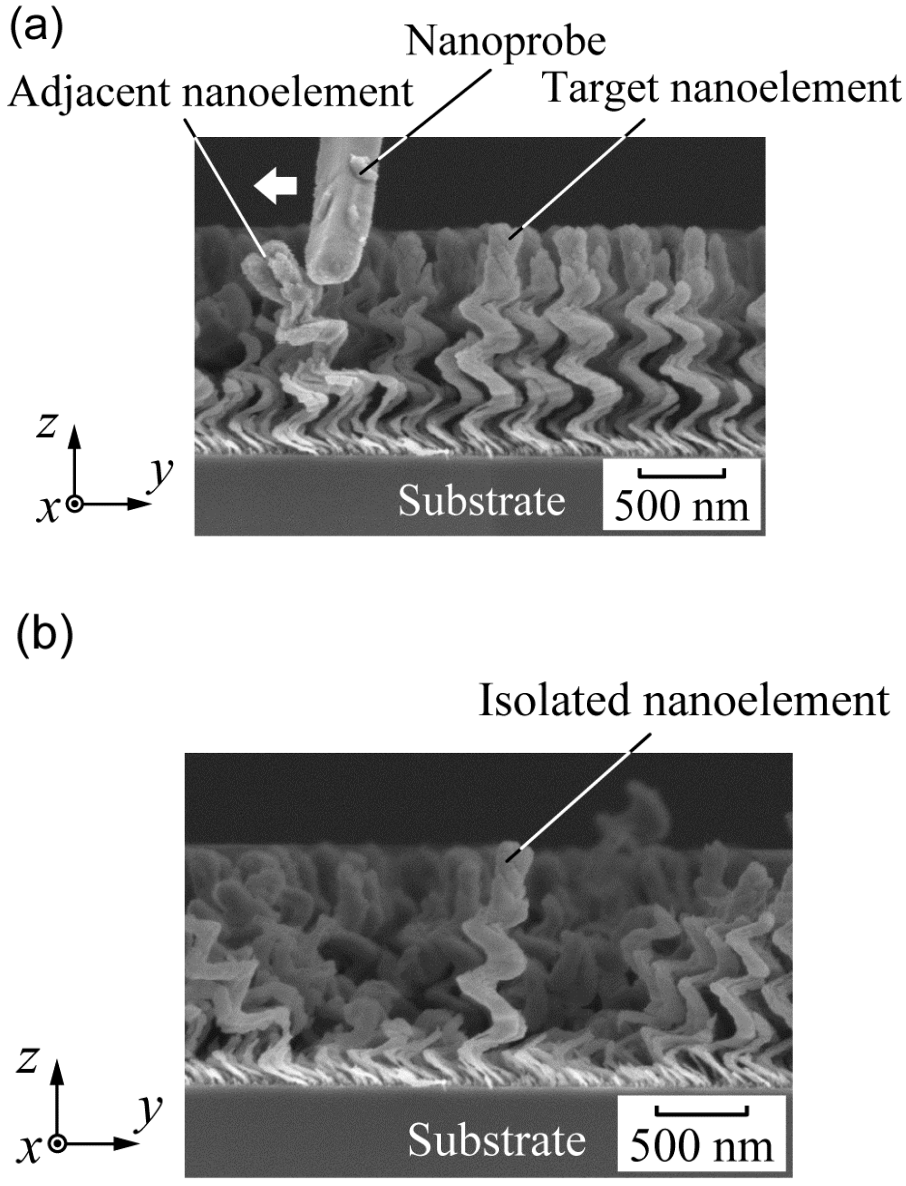

Fig. 3. Extraction of a single Si nanospring (a) by removal of adjacent nanoelements around the target nanoelement using a nanoprobe. (b) Individual Si nanospring isolated.

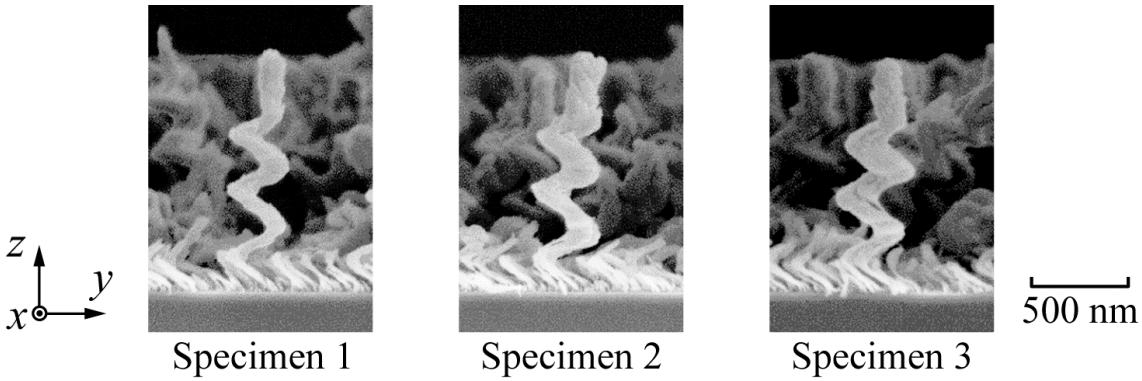

Fig. 4. SEM images of three nanospring specimens.

4.2.2 Experimental facility and conditions

Tensile experiments are conducted using SEM (Hitachi High-Tech, SU-8230) with a specimen stage and two manipulators (Kleindiek, MM3A-EM), as shown in Fig. 5(a). One of the manipulators has a needle-shaped tungsten nanoprobe (GGB Industries Inc, PT-14-6705-B) (Fig. 5(b)), while the other is equipped with a force sensor (Seiko instruments Inc, NPX1CTP003) (Fig. 5(c)). The sensitivity of the force sensor is 0.02 μN. The specimen substrate is fixed on the specimen stage, which can be rotated to give the best angle for observation and loading. Nanosprings adjacent to the target nanospring are mechanically bent and removed by operation of the nanoprobe, as shown in Fig. 3(a). The operation takes about 5 minutes for each specimen.

Loading experiments are conducted using the other manipulator with the force sensor. Both manipulators have rotational freedom (*y*-*z* and *x*-*y* planes) and sliding freedom (*y* direction), which ensures correct tensile alignment on the specimen along the vertical center axis of the nanospring during the loading process. The resolution of the manipulators for stretching and rotating is 0.25 nm and 10^{-7} rad, respectively. The force sensor can measure tensile or compression forces.

The loading tip is adhered to the top of a nanospring after a conductive epoxy adhesive (Kleindiek, SEM GLU), which was dropped on the side of specimen stage beforehand (See Fig. 6), is dipped. The adhesive is hardened by electron beam irradiation at 2.0 kV for 5 min, which is sufficient for tensile loading of a single nanospring.

A tensile force is applied to the specimen by imposing a displacement on the top end of the single nanospring, while the bottom end is fixed on the substrate, as shown in Fig. 6. A small preliminary load is applied to the nanospring, and the loading alignment is

carefully tuned using the ability of the manipulator to rotate and slide, while the specimen is monitored from the SEM image. Tensile experiments are conducted at a displacement rate $d\delta_v/dt$ of 2 nm/s. The elongation of the entire single nanospring, which is the displacement increment between the bottom end of nano-helix and the original point, as well as that in local regions of the nanospring are measured using 2D-motion analysis software (Library, Move-tr/2D) on the basis of continuous SEM observations. The specimen fracture can be determined based on the monitoring of applied load and the *in situ* SEM observation.

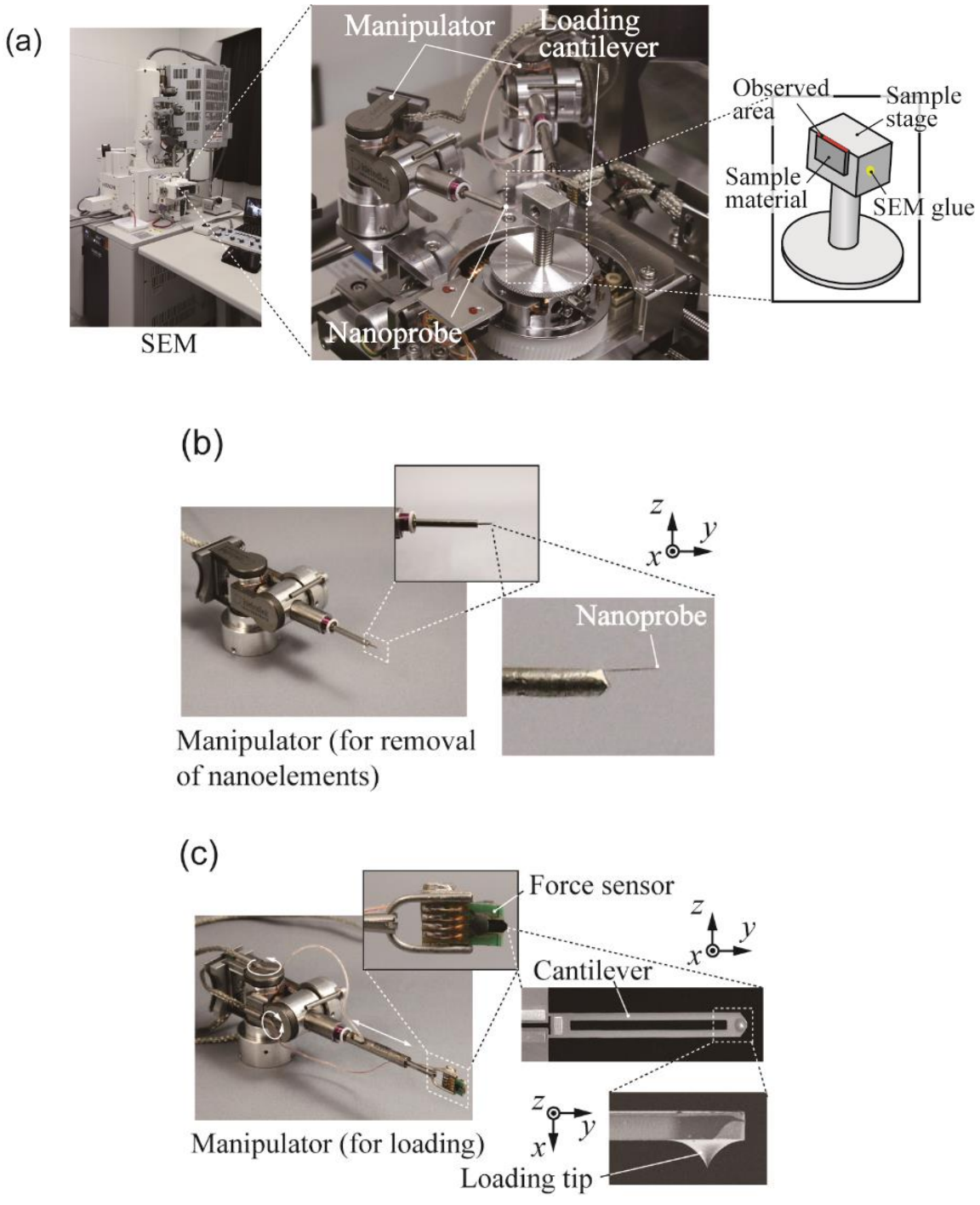

Fig. 5. Experimental equipment, (a) the testing system and specimen stage, (b) the manipulator and nanoprobe, and (c) the manipulator and force sensor, and micrographs showing details of the force sensor.

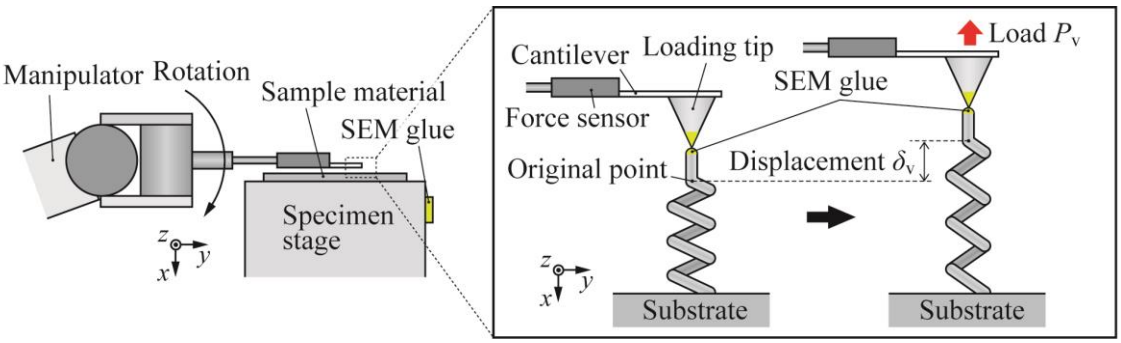

Fig. 6. Schematic illustration of tensile testing with a single nanospring.

4.3 Experimental results and discussion

4.3.1 Tensile properties

Figure 7 shows the load versus displacement (P_v-δ_v) curve for Specimen 1 and snapshot micrographs taken from the *in situ* SEM video during tensile testing at loading forces of 0 μN (A), 0.26 μN (C), 0.80 μN (D) and after fracture (E). The P_v and δ_v are plotted based on the output data from the load sensor and the 2D-motion analysis software, respectively. The average stiffness of a single nanospring is 3.8 N/m and the fracture displacement is 256 nm, which represents an apparent fracture strain of $\varepsilon'_f = 3.03\times10^{-1}$. It should be noted that there is a jump in the P_v-δ_v relation between points B and C indicated on the curve, where the slope changes after the jump, indicating a decrease in stiffness. The cause of this jump is discussed in the following section. After δ_v = 150 nm, the gradient increases. The height of the bottom zone of the nanospring is extended eminently by the concentrated deformation, as shown in Fig. 7(b). The increase in stiffness is attributed to the change in the shape of the elongated spring. Fracture occurs near the bottom of the spring where the spring wire diameter is smaller. Figure 7(c) shows SEM images of the nanospring before and after fracture. Based on the difference between the length of the nanospring before and after experiment, the residual deformation, δ_r, is obtained. Although micrograph (E) shows little change in the shape, a high residual displacement of 133 nm is observed at fracture, which is almost half of the fracture displacement. This signifies that a large plastic deformation occurs in the amorphous silicon spring under tension.

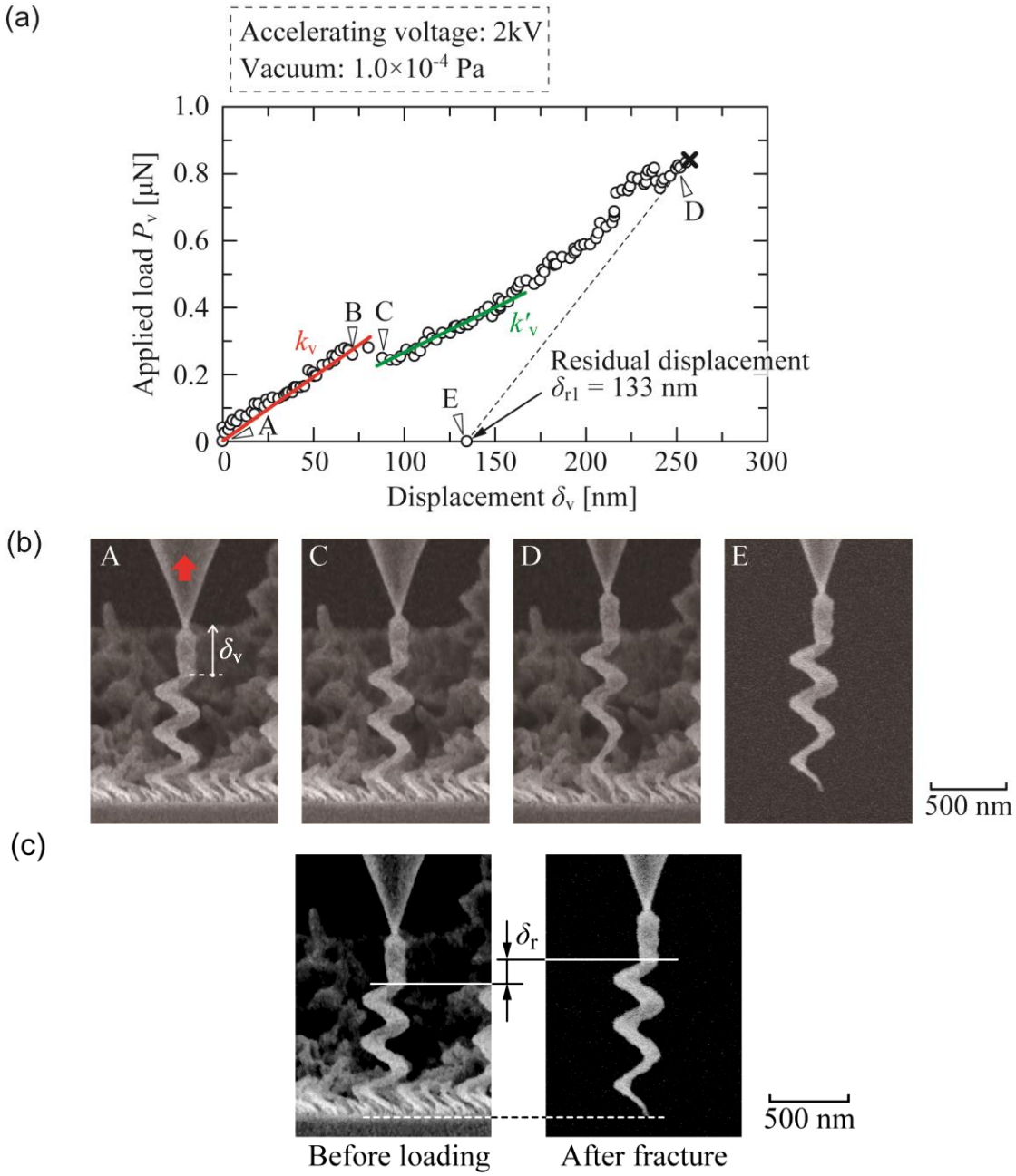

Fig. 7. Deformation and fracture behavior for Specimen 1 under monotonic tension; (a) load versus displacement curve, (b) microscopic features of the nanospring under tensile loads at F_v = (A) 0 μN, (C) 0.26 μN, and (D) 0.80 μN, and (E) after fracture, and (c) comparison of the nanospring before and after experiment.

Figure 8 shows P_v-δ_v curves for the three specimens tested. The springs clearly have different tensile behavior, even though they all are isolated on the same GLAD substrate. Specimen 3 is stiffer than the others, while the overall shapes of Specimens 2 and 3 are similar. The residual displacement indicates differences in the plastic deformation among the springs. There are distinct differences in terms of the fracture load and elongation among the springs, which means that both the deformation and fracture behavior are highly dependent on the individual spring. Moreover, careful observation reveals a jump in the P_v-δ_v curves for all specimens, although the load at each jump is different. The mechanical behavior reported for GLAD films in previous research is for loading of many springs [22, 24-26], so that the strength calculated is the average value. This is the first report to present distinct differences in the mechanical behavior of individual springs in a GLAD film.

Table 1 gives the dimensions for each nanospring. Each spring possesses a different shape although they are isolated on the same GLAD film, which emphasizes the necessity to determine the tensile processes of individual nanosprings with different strengths, as shown in Fig. 8.

Table 1 Dimensions of specimens (units: nm).

	d_{I}	d_{II}	d_{III}	D_{I}	D_{II}	D_{III}	h_{I}	h_{II}	h_{III}	h_{s}
Specimen 1	49	84	87	128	148	187	308	292	243	843
Specimen 2	79	99	138	138	138	167	293	288	239	820
Specimen 3	89	118	138	133	165	148	286	296	242	824

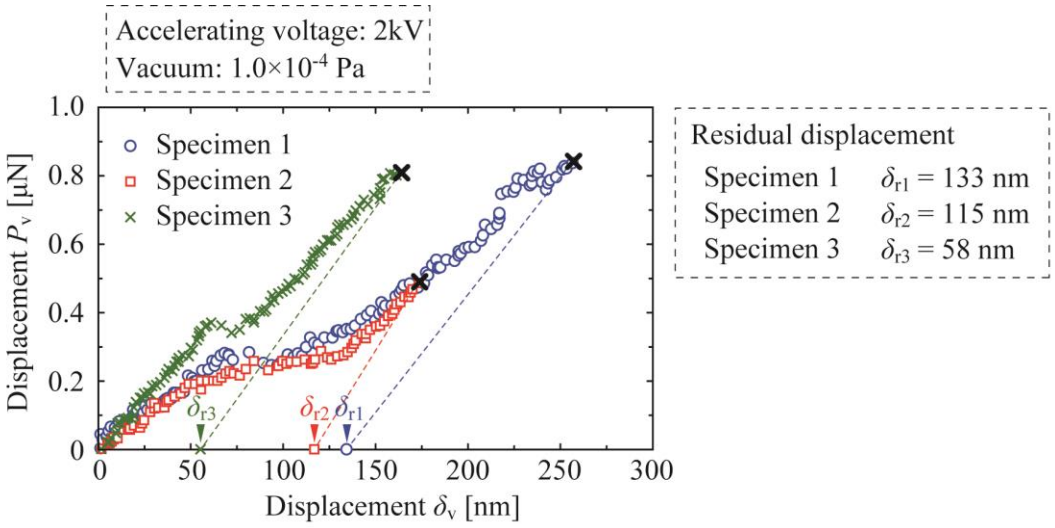

Fig. 8. Load-displacement curves for three specimens under tension.

4.3.2 Deformation in the bottom zone.

Figure 4 and Table 1 show that the shape and size of each nanospring changes from the bottom to the top, which suggests that the deformation is not uniform. An advantage of *in situ* SEM video observation is that such nonuniform deformation can be investigated in detail. Here, a single spring is divided into three zones (I, II and III) and the displacement in each zone is measured under a load. Figure 9 shows the P_v-δ_v curve in the different zones of Specimen 1. As expected from the shape, where the turn diameter *D*, and the spring wire diameter *d*, are both smaller in the bottom turn, the top is stiffer while the bottom is more flexible. The stiffness in each zone from the bottom to the top is approximately $k_{v1\text{-}I}$ = 4.8 N/m, $k_{v1\text{-}II}$ = 9.8 N/m and $k_{v1\text{-}III}$ = 53.0 N/m, which confirms that the deformation of the spring is mainly governed by the bottom zone.

The residual deformation after fracture can be measured from the SEM image, and the apparent residual strain after fracture from the bottom to top are $\varepsilon'_{r1\text{-}I} = 1.58\times10^{-1}$, $\varepsilon'_{r1\text{-}II} = 0$ and $\varepsilon'_{r1\text{-}III} = 0$. Thus, during the tensile test, only the bottom zone is plastically deformed, while the other zones exhibit elastic deformation; the bottom zone dominates the deformation process and the concentrated strain results in fracture due to the nonuniform thickness in this zone.

There is a jump in the P_v-δ_v curve in Fig. 9(a) that corresponds to that in Fig. 7(a), which confirms that it is associated with the bottom zone. Careful review of this zone before and after the jump reveals that the spring is initially connected to the substrate by two legs, as schematically illustrated in Fig. 9(d) and one of these legs breaks at the jump. As only one leg is then supporting the spring, the stiffness decreases. While numerous nuclei are formed at the early stage of spring growth during the GLAD technique, many stop growing, which leaves incomplete spring frameworks on the

substrate as shown in Fig. 1. Some neighboring nuclei connect with each other and a nanospring is formed on the connected nuclei. The jump in the P_v-δ_v curve is caused by a break in the weaker connection. The same mechanism is observed for Specimens 2 and 3; therefore, it appears that the presence of multiple connection legs is common, and this plays a dominant role in the elastic properties of the spring during the early stage of tension.

From careful examination of the bottom zone in Specimens 1 to 3, Specimen 3 is identified as having the thickest connection at the root (see Fig. 4). This may be the reason why Specimen 3 had the highest stiffness during the early stage of deformation, as shown as Fig. 8. The mechanical properties are significantly affected by this subtle difference in spring geometry. However, as the back side connection between the spring and nuclei cannot be observed using SEM, a qualitative discussion is not possible at this stage.

(a)

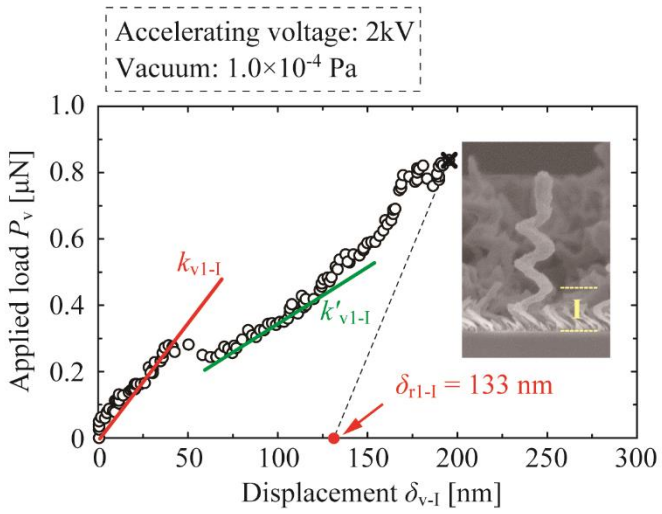

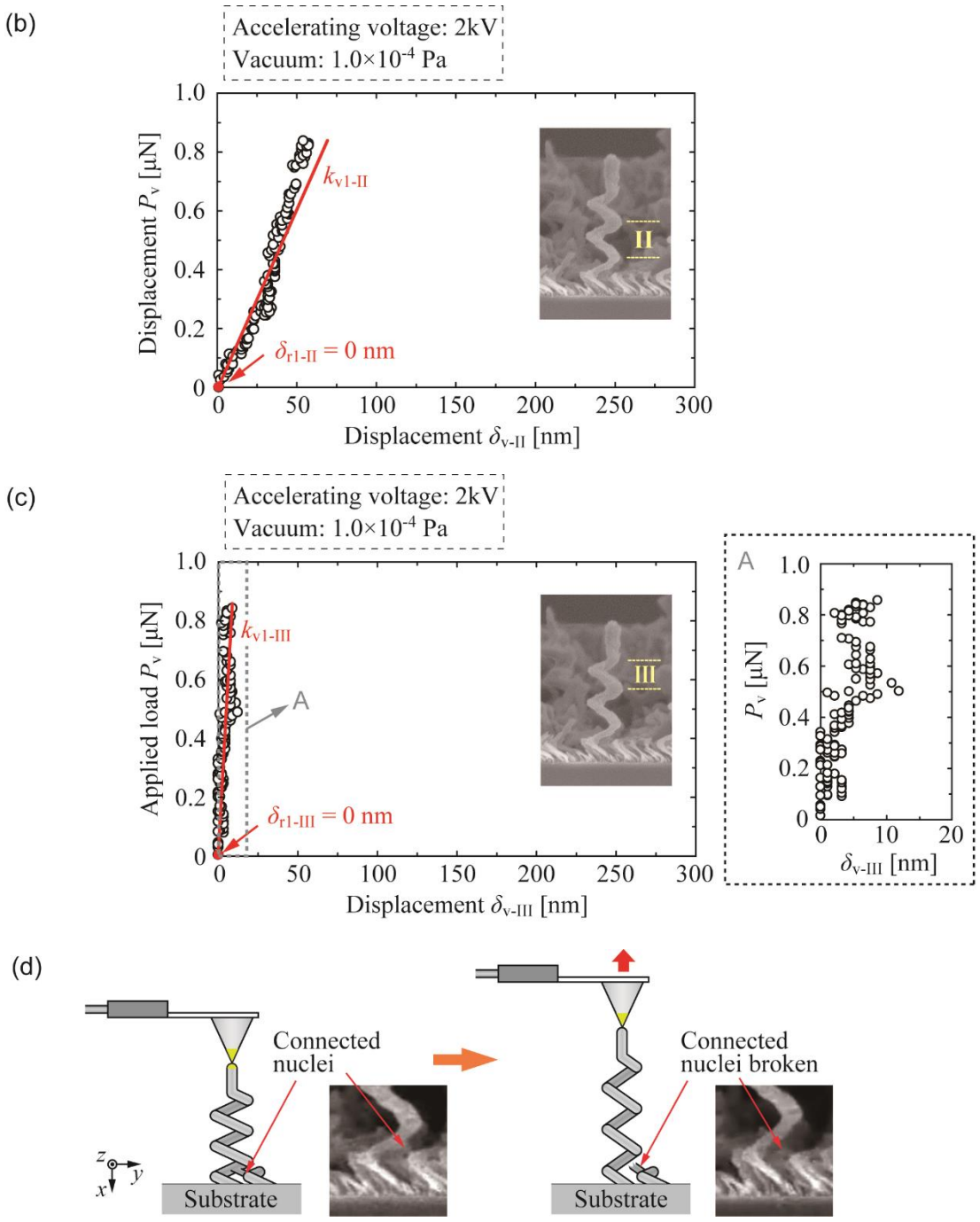

Fig. 9. Load-displacement curves for Specimen 1; (a) first (lower) zone, (b) second (middle) zone, (c) third (upper) zone, and (d) schematic illustrations of specimen separation at connection nuclei.

4.3.3 Elastic behavior

Based on the theoretical equation of a helical spring, the deformation stiffness of zones I, II and III of nanospring is examined. The cross-sectional shape of nanospring is approximated by a circle. Elastic theory states that a helical spring has a vertical stiffness, $k_{v,th}$ [29]:

$$k_{v,th} = \frac{Gd^4}{8D^3 n}\left[1 - \frac{3d^2}{16D^2} + \frac{3+\nu}{2(1+\nu)}(\tan\alpha)^2\right]^{-1} \quad (1)$$

where G and ν are the shear modulus and Poisson's ratio, respectively, and d, D, n and α are the spring wire diameter, the coil diameter of the helical spring, the number of turns, and the pitch angle of the spring, respectively. It should be noted that this is an approximate estimate since the wire diameter of nanospring is gradually broaden toward the top and the boundary conditions at the ends are not strictly same. Figure 10 shows the relationship between the stiffness experimentally obtained and $k_{v,th}/G$ for the second and third zones in each specimen. Since the G of the amorphous Si of nanospring deposited by GLAD is unknown, $k_{v,th}/G$ is used as a parameter of the horizontal axis. Here, n = 1 in each zone and the stiffness is measured under low load conditions. The stiffness is approximately proportional to $k_{v,th}/G$, so that relation (1) governs the deformation in most areas of the spring, except the bottom zone. This signifies that the deformation stiffness is governed by the nano-helix shape.

It should be noted that the stiffness is dependent not only on the zone, but also the nano-helix shape. Figure 10 indicates that the fluctuation in nano-helix shape, as listed in Table 1, causes the difference in the stiffness, which is consistent with elastic theory.

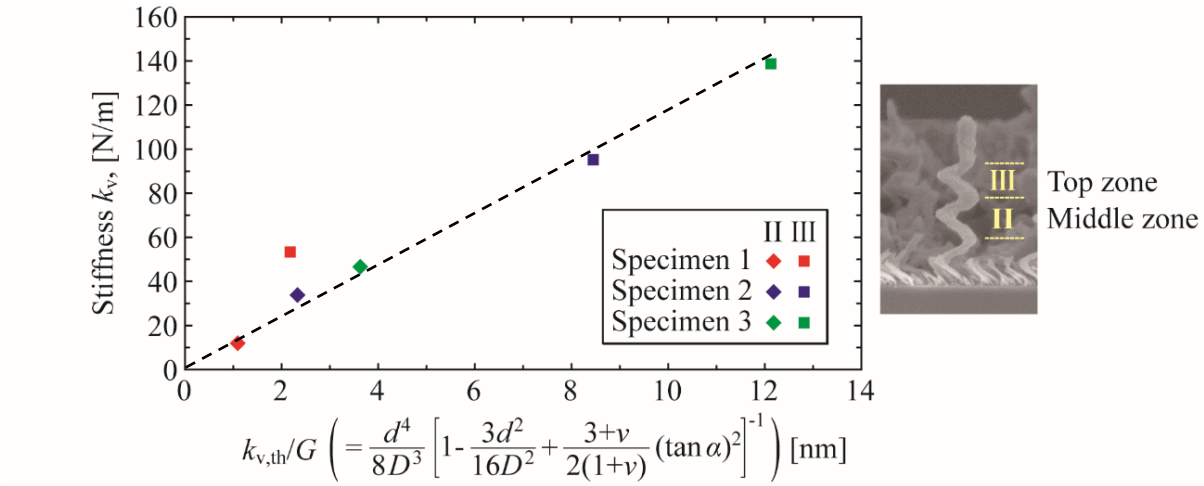

Fig. 10. Relationship between stiffness k_v, and $k_{v,th}/G$ for the first and second zone of the specimens.

Elastic theory also indicates that the maximum shear stress τ_{max}, in a spring wire is given by [34]:

$$\tau_{max} = \frac{8P_v D}{\pi d^3}\left[1 + \frac{5d}{4D} + \frac{7}{8}\left(\frac{d}{D}\right)^2\right] \quad (2)$$

Figure 11 shows the calculated τ_{max} and ε'_r for each zone in the nanosprings. There is no apparent residual strain ε'_r when τ_{max} is less than 0.8 GPa, whereas ε'_r increases significantly above 0.8 GPa. This indicates that the yield stress of the amorphous Si for nanospring is estimated to be around 0.8 GPa.

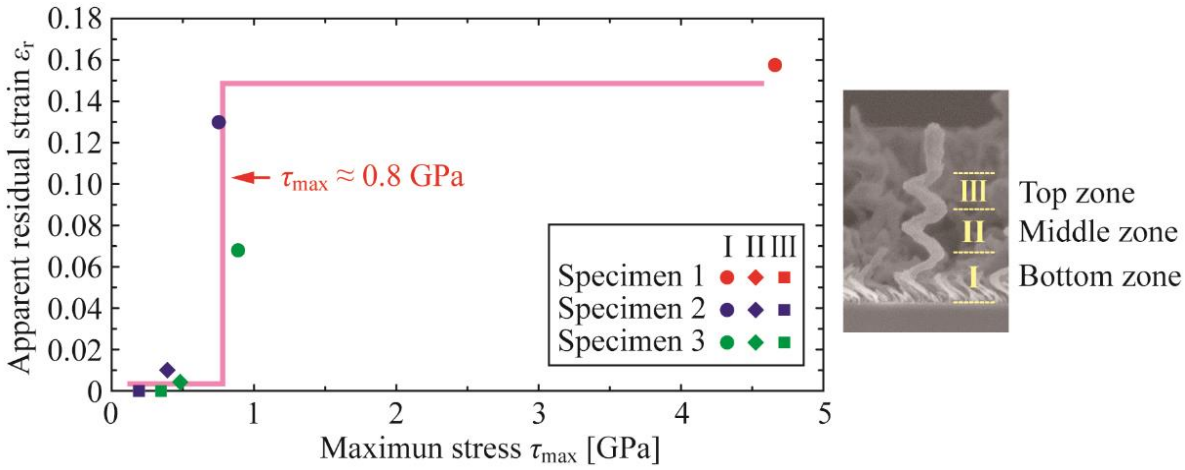

Fig. 11. Distribution of maximum shear stress τ_{max}, and apparent residual strain ε'_r, for the different zones of the specimens.

4.4 Conclusions

In this chapter, a tensile testing method was developed for measuring the mechanical properties of single nanoelements extracted from an aggregate layer under *in situ* SEM observation. Specimens were isolated from amorphous silicon nanosprings prepared by the GLAD technique. The results obtained are summarized as follows:

1. Three single nanosprings were successfully isolated using a nanoprobe, and tension was applied to the top of the springs using a probe with a load sensor until failure occurred. The deformation and fracture processes were continuously monitored using *in situ* SEM during the tensile test.

2. Each nanospring exhibited different load-displacement relations, even though they are from the same GLAD layer. The *in situ* SEM observation confirmed that this was mainly due to differences in spring geometry. In particular, the connected nuclei at the spring bottom had a significant effect on the stiffness during the early stage of tensile loading.

3. The spring wire diameter and the coil diameter varied between the top and bottom of a spring; therefore, the deformation process was nonuniform. However, elastic spring theory was found to be approximately valid for the deformation characteristics in the elastic stage, where the deformation was mainly governed by the shape of the nanoelement.

4. The bottom zone of the nanospring, which had the smallest wire and coil diameters, played a dominant role in plastic deformation and failure occurred here. The yield stress of the nanosprings was estimated to be approximately 0.8 GPa based on the

maximum shear stress of the spring wire.

References in chapter 4

[1] Zhou, C. M., and D. Gall. "Development of two-level porosity during glancing angle deposition." Journal of Applied Physics 103.1 (2008): 14307.

[2] Fuhrmann, Bodo, et al. "Ordered arrays of silicon nanowires produced by nanosphere lithography and molecular beam epitaxy." Nano letters 5.12 (2005): 2524-2527.

[3] G. Kipshidze, B. Yavich, A. Chandolu, J. Yun, V. Kuryatkov, I. Ahmad, D. Aurongzeb, M. Holtz, H. Temkin, "Controlled growth of GaN nanowires by pulsed metalorganic chemical vapor deposition." Appl. Phys. Lett. 86 (2005) article number: 033104.

[4] Li, Yunfeng, et al. "Bioinspired silicon hollow-tip arrays for high performance broadband anti-reflective and water-repellent coatings." Journal of Materials Chemistry 19.13 (2009): 1806-1810.

[5] P. Mohan, J. Motohisa, T. Fukui, "Controlled growth of highly uniform, axial/radial direction-defined, individually addressable InP nanowire arrays." Nanotech. 16 (2005) 2903-2907.

[6] Burek, Michael J., and Julia R. Greer. "Fabrication and microstructure control of nanoscale mechanical testing specimens via electron beam lithography and electroplating." Nano letters 10.1 (2009): 69-76.

[7] S.D. Hersee, X.Y. Sun, X. Wang, "The Controlled Growth of GaN Nanowires."

Nano Lett. 6(8) (2006) 1808-1811.

[8] W. Lee, M.C. Jeong, M.J. Kim, J.M. Myoung, "Field emission characteristics of ZnO nanoneedle array cell under ultraviolet irradiation." Phys. Lett. A 370 (2007) 345-350.

[9] Y. Lai, C. Lin, H. Wang, J. Huang, H. Zhuang, L. Sun, "Superhydrophilic–superhydrophobic micropattern on TiO_2 nanotube films by photocatalytic lithography." Electrochem. Commun. 10 (2008) 387-391.

[10] K. Robbie, M.J. Brett, A. Lakhtakia, "First thin film realization of a helicoidal bianisotropic medium." J. Vac. Sci. Technol. A 13 (1995) 2991-2993.

[11] K. Robbie, M.J. Brett, A. Lakhtakia, "Chiral sculptured thin films." Nature 384 (1996) 615-616.

[12] R. Messier, V.C. Venugopal, P.D. Sunal, "Origin and evolution of sculptured thin films." J. Vac. Sci. Technol. A 18 (2000) 1538-1545.

[13] M. Suzuki, Y. Taga, "Integrated Sculptured Thin Films." Jpn. J. Appl. Phys. 40 (2001) L 358-L359.

[14] G.D. Dice, M.J. Brett, D. Wang, J.M. Buriak, "Fabrication and characterization of an electrically variable, nanospring based interferometer." Appl. Phys. Lett. 90 (2007) article number: 253101.

[15] M.F. Schubert, J.Q. Xi, J.K. Kim, E.F. Schubert, "Distributed Bragg reflector consisting of high- and low-refractive-index thin film layers made of the same material." Appl. Phys. Lett. 90 (2007) article number: 141115.

[16] M.M. Hawkeye, M.J. Brett, "Glancing angle deposition: Fabrication, properties, and applications of micro- and nanostructured thin films." J. Vac. Sci. Technol. A 25 (2007) 1317-1335.

[17] J.G. Fan, J.X. Fu, A. Collins, and Y. P. Zhao, "The effect of the shape of nanorod arrays on the nanocarpet effect." Nanotechnology, 19(4) (2008) article number: 045713.

[18] S.P. Fernando, A.L. Elias, and M.J. Brett, "Mechanical properties of helically perforated thin films." Journal of materials research 21(5) (2006) 1101-1105.

[19] J. Lintymer, N. Martin, J.M. Chappe, P. Delobelle, J. Takadoum, "Influence of zigzag microstructure on mechanical and electrical properties of chromium multilayered thin films." Surf. Coat. Technol. 180-181 (2004) 26-32.

[20] J. Potocnik, M. Nenadovic, B. Jokic, M. Popovic, and Z. Rakocevic, "Properties of Zig-Zag Nickel Nanostructures Obtained by GLAD Technique." Science of Sintering, 48(1) (2016), 51-56.

[21] K. Robbie, J.C. Sit, M.J. Brett, "Advanced techniques for glancing angle deposition." J. Vac. Sci. Technol. B 16 (1998) 1115-1122.

[22] C.M. Zhou, D. Gall, "The structure of Ta nanopillars grown by glancing angle deposition." Thin Solid Films 515 (2006) 1223-1227.

[23] S.V. Kesapragada, D. Gall, "Anisotropic broadening of Cu nanorods during glancing angle deposition." Appl. Phys. Lett. 89 (2006) article number: 203121.

[24] A.F. da Fonseca, D.S. Galvao, "Mechanical Properties of Nanosprings." Phys. Rev.

Lett. 92(17) (2004) article number: 175502.

[25] Wang, Jian, et al. "Growth of Y-shaped nanorods through physical vapor deposition." Nano letters 5.12 (2005): 2505-2508.

[26] A.F. da Fonseca, D.S. Galvao, "Mechanical Properties of Nanosprings." Phys. Rev. Lett. 92(17) (2004) article number:175502.

[27] T. Sumigawa, H. Hirakata, M. Takemura, S. Matsumoto, M. Suzuki, T. Kitamura, "Disappearance of Stress Singularity at Interface Edge due to Nanostructured Thin Film." Eng. Fract. Mech.75 (2008) 3073-3083.

[28] T. Sumigawa, T. Sueda, Y. Futamura, M. Suzuki, T. Kitamura, "Effect of interface layer consisting of nanosprings on stress field near interface edge." Eng. Fract. Mech. 76 (2009) 1336-1344.

[29] H. Hirakata, S. Matsumoto, M. Takemura, M. Suzuki, T. Kitamura, "Anisotropic deformation of thin films comprised of helical nanosprings." Int. J. Solids Struct. 44(11-12) (2007) 4030-4038.

[30] M.W. Seto, B. Dick, M.J. Brett, "Microsprings and microcantilevers: studies of mechanical response." J. Micromech. Microeng. 11 (2001) 582-588.

[31] M.W. Seto, K. Robbie, D. Vick, M.J. Brett, L. Kuhn, "Mechanical response of thin films with helical microstructures." J. Vac. Sci. Technol. B 17 (1999) 2172-2177.

[32] D.L. Liu, D.X. Ye, F. Khan, F. Tang, B.K. Lim, R.C. Picu, G.C. Wang, T.M. Lu, "Mechanics of Patterned Helical Si Springs on Si Substrate." J. Nanosci. Nanotech. 3(6) (2003) 492-495.

[33] C. Gaire, D.X. Ye, F. Tang, R.C. Picu, G.C. Wang, T.M. Lu, "Mechanical Testing of Isolated Amorphous Silicon Slanted Nanorods." J. Nanosci. Nanotech. 5(11) (2005) 1893-1897.

[34] C.J. Ancker, J.N. Goodier, "Pitch and curvature corrections for helical springs." J. Appl. Mech. 25 (1958) 466-470.

Chapter 5 Conclusions

Nanostructured thin film consisting of discretely nano-sized three-dimensional nanosprings has attracted considerable attention for the promising potential application in advanced electronic devices due to its unique physical properties. Although the glancing angle deposition technique (GLAD) has been developed to fabricate thin films consisting of discretely nano-sized three-dimensional elements, there are still some unclear points. For instance, some critical issues in the precise fabrication and the exact evaluation of mechanical properties of nanospring thin films are still required to be clearly investigated. Therefore, in this thesis, a novel experimental method basing on the precise control of substrate temperature is developed to fabricate the nanospring thin films of low-melting metals, and the substrate temperature effect on the morphology of nanospring thin films is clarified. In addition, the deformation and fracture behaviors of nanospring thin films as well as the individual nanospring are investigated by experimental and numerical studies. The obtained results are summarized as follows.

In chapter 2, a developed GLAD system which can precisely control the temperature of substrate during glancing angle deposition is developed to make films consisting of low melting temperature metal nanoelements with a controlled shape (helix) and to explore the substrate temperature for controlling the nanoshapes. This novel GLAD system capable of both cooling a substrate and measurement of its temperature is used to form thin films consisting of arrays of Cu and Al nanosprings on silicon substrates by maintaining the substrate temperature at $T_s/T_m<0.22$ (T_s is the substrate temperature and T_m is the melting temperature of target material). The critical homologous temperature

(T_s/T_m) to produce Cu and Al nanosprings corresponds to the transitional homologous temperature between zones I and II in the structure zone model for the solid film, where surface diffusion becomes dominant. In addition, the X-ray diffraction analysis indicated that the Cu and Al nanospring thin films were composed of coarse oriented grains with diameters of several tens of nanometers.

In chapter 3, the vertical compression loading is conducted to investigate the elastic limit of the thin film consisting of nickel helical nanosprings by an atomic force microscope (AFM). As a helical element has large reversible deformation limit in general, a characteristic behavior is expected on the yielding of the film. The load versus displacement curves indicate that the nickel nanosprings thin film has outstanding elastic limit. The apparent yield strain is evaluated as $\varepsilon_Y' = 5.2 \sim 6.2\times10^{-2}$, which is around 200 times of that in bulk nickel ($\varepsilon_Y = 0.29 \sim 0.44\times10^{-3}$). After comparing the maximum shear stress in the helical spring and the solid film, the shape effect (helical shape) is only around 10 ~ 20 times stemmed from the difference in the stress condition (torsion). The origin of difference is attributed to the size effect of nanosprings, as nano-scale metals have higher yield strain than that of bulk counterpart because of the difference in the understructure morphology. The combination of shape effect and size effect brings about the giant elastic limit on the film.

In chapter 4, a tensile testing method is developed for measuring the mechanical properties of single nanoelements extracted from an aggregate layer under *in situ* SEM observation. Specimens are isolated from amorphous silicon nanosprings prepared by

GLAD technique. *In situ* observation reveals that the single nanospring undergoes a large longitudinal elastic elongation until fracture (about 40% of the fracture displacement) due to the helical shape. At the early stage of deformation, there is a jump in the load-displacement relation due to partial breaking of the connected legs at the root of the nanospring. The tension induces plastic deformation and fracture at the bottom zone where the wire diameter is smaller. Examination based on the element geometry at local zones indicates that deformation in the elastic stage is governed by the element shape. The yield stress of the amorphous silicon for nanospring is estimated to be approximately 0.8 GPa.

Publication and conferences

Publication

[1] "Outstanding elastic limit of a thin film composed of nickel nanosprings. Journal of Nanoscience and Nanotechnology"

Shaoguang Chen, Kazuya Iwata, Takashi Sumigawa, Takayuki Kitamura
(*Journal of Nanoscience and Nanotechnology*, Vol. 17, pp. 828-832, 2017)

[2] "Substrate temperature control for the formation of metal nanohelices by glancing angle deposition"

Takashi Sumigawa, Hisashi Tanie, Atsushi Sakurai, Kazuya Iwata, Shaoguang Chen, Takayuki Kitamura
(*Journal of Vacuum Science & Technology* A, Vol 33.6, pp. 060609, 2015)

[3] "*In situ* Observation of Tensile Behavior in a Single Silicon Nano-helix"

Takashi Sumigawa, Shaoguang Chen, Tetsuya Yukishita, Takayuki Kitamura
(*Thin Solid Films*, under review)

International conferences

[1] "*In situ* Observation of Tensile Behavior in a Single Silicon Nanospring"

Shaoguang Chen, Takashi Sumigawa, Tetsuya Yukishita, Takayuki Kitamura
Asia-Pacific Conference on Fracture and Strength 2016
(Toyama, Japan, 2016.9)

Acknowledgements

This research work was conducted under the supervision of my supervisor Professor Takayuki Kitamura. I would like to convey my sincerest appreciation for his earnest guidance in the process of this work. His support, understanding, encouragement, enlightening discussion, and precious advices during my time in the laboratory are greatly appreciated and admired. What I have learned under his supervision is huge and will greatly extend my research work in future.

I would like to sincerely thank Professor Shinji Nishiwaki and Professor Masaki Hojo for their helpful advices and illuminating comments. The time and energy they spent on evaluating and reviewing this work are sincerely appreciated.

I wish to thank Associate Professor Takashi Sumigawa and Assistant Professor Takahiro Shimada for their fruitful discussions, helpful advices, and constructive suggestions for my study.

I would like to thank Dr. Yabin Yan (China Academy of Engineering Physics), Dr. Tao Xu (Kyoto University), Dr. Kai Huang (Harbin Institute of Technology), Professor Jianshan Wang (Tianjin University), Professor Hongjun Yu (Harbin Institute of Technology) and all members of Material Science Laboratory for their helpful discussion and inspiring suggestions. Especially, I would like to thank my Japanese colleagues in this lab for their considerable help in daily life, which makes the author to have a smoother life in Japan and get a deeper understanding in Japanese cultures.

I would like to convey my sincerely appreciation to my parents, and my younger sister for their continuous support and encouragement.

Last but not least, I also would like to appreciate the financial support of China Scholarship Council (CSC Scholarship) during my doctor course study.